Structural and Luminescence Characterization of Europium-doped Niobium Germanate Glasses and Glass-Ceramics: Novel insights from ^{93}Nb Solid-State NMR Spectroscopy

Lia Mara Marcondes[1,+,*], Henrik Bradtmüller[2,+], Sabrina Nicoleti Carvalho dos Santos[3], Lucas Konaka Nolasco[3], Cleber Renato Mendonça[3], Silvia Helena Santagneli[1], Gael Yves Poirier[4], Marcelo Nalin[1*]

[1] Instituto de Química, Universidade Estadual Paulista Júlio de Mendonça Filho, Araraquara, SP, Brazil

[2] Departamento de Engenharia de Materiais, Universidade Federal de São Carlos, São Carlos, SP, Brasil

[3] Instituto de Física de São Carlos, Universidade de São Paulo, São Carlos, SP, Brazil

[4] Grupo de Química de Materiais, Universidade Federal de Alfenas, Campus Poços de Caldas, Poços de Caldas, MG, Brazil

(*) corresponding author.

(+) These authors contributed equally to this work.

E-mail: lia-marcondes@hotmail.com; marcelo.nalin@unesp.br

Mail address: Instituto de Química, Universidade Estadual Paulista Júlio de Mendonça Filho – UNESP, Rua Prof. Franscisco Degni, 55 – Quitandinha – Araraquara/SP, Brazil – CEP 14800-060

Highlights

- Direct evidence ^{93}Nb chemical shift is sensitive to configuration of second-coordination sphere
- First NMR spectroscopic distinction of different NbO_6 species in niobium germanate glasses thanks to very-fast MAS and novel 3QMAS pulse sequence;
- Luminescent europium ions exploited as sensitive probes for elucidating the glass-to-crystal transition and giving more evidence for formation of NbO_6 clusters;
- We demonstrate the feasibility of creating of photonic waveguides by femtosecond laser inscription;

Graphical abstract

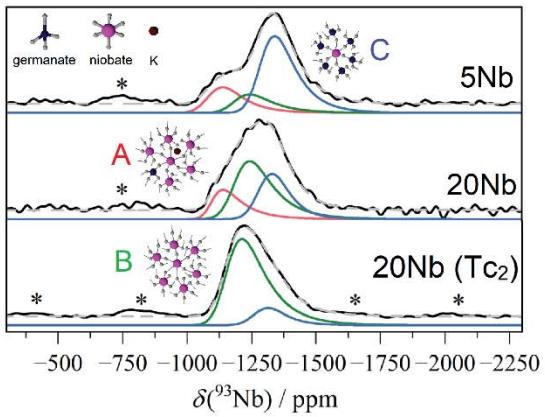

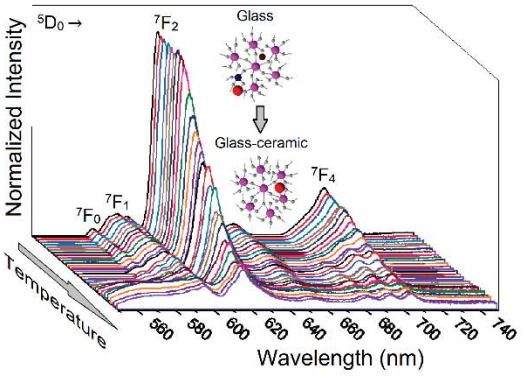

Abstract

A thorough understanding of network former roles in optical glasses and glass-ceramics, as well as structural environments of luminescent rare-earth atoms, is paramount to assessing their suitability and effectiveness as components for fully-optical integrated devices. The present contribution sheds light on the overall poorly understood structural role of Nb_2O_5 in oxide glasses and offers a rationale for the luminescence changes concomitant to the heat-treatment induced glass-to-crystal transition in niobium germanate glasses. To this end, results from ^{93}Nb nuclear magnetic resonance (NMR), Raman, and Eu^{3+} ion based luminescence spectroscopies as well as 3D micromanufacturing are reported for glasses and glass-ceramics in the system $(89.9\text{-}x)GeO_2\text{-}xNb_2O_5\text{-}10K_2O\text{-}0.1Eu_2O_3$. Thanks to very-fast ^{93}Nb magic-angle spinning (MAS) and a novel excitation scheme for Triple-quantum (TQ)MAS solid-state NMR spectroscopy distinct $Nb(OGe)_{6-y}(ONb)_y$ species were identified for the first time: at low Nb concentrations structural units with rather low y-values are formed, reaching down to isolated $Nb(OGe)_6$ units – next to units bearing non-bridging oxygen atoms; at intermediate Nb contents and beyond, structural units with increasingly higher y-values up to $Nb(ONb)_6$ are found, resembling the local environments found in crystalline Nb_2O_5. After the glass-to-crystal transition the Nb local environment mainaints a high degree of disorder while some residual glass remains. Moreover, photoluminescence spectroscopy of the europium probes suggests the rare-earth ions are preferentially incorporated into high y-value $Nb(OGe)_{6-y}(ONb)_y$ polyhedra based on spectral features such as the phonon sideband, the $^5D_0 \rightarrow {}^7F_2/{}^7F_1$ ratio, and split 4f bands. Finally, femtosecond laser microfabrication of waveguides was successful in the presented europium-doped niobium germanate glasses, making them promising candidates for further studies as photonic devices.

Keywords: ^{93}Nb solid-state NMR; europium probe; glass crystallization; photonic waveguides.

1. Introduction

All-optical signal processing is of considerable importance in fundamental research and applied technology, carrying the promise of enhanced overall circuit speeds which are usually limited by the responses time of electronic devices [1,2]. Waveguides employed as building blocks in optical integrated circuits play a critical role in ultra-fast data transmission and device miniaturization [3]. Rare-earth doped micro-waveguides in glass material with nonlinear, magneto-optical properties, can be employed as isolators [4], rotating modules [4], switches and modulators [5], and high-performance active gain devices [3]. Alkali niobium-germanate glasses are interesting candidates for these applications [6], based on their wide transparency window ranging from 0.4 μm to 5 μm. Furthermore, their highly nonlinear refractive indices [7] combined with their low cutoff phonon energy (< 800 cm^{-1}), which is significantly lower than for conventional silicate (< 1150 cm^{-1}) or pure germanate (< 900 cm^{-1}) glasses [8], greatly enhance rare-earth photoluminescence efficiency [9,10]. In order to fine-tune these optical properties, the composition-structure-property relationships in the system must be better understood. The structure of niobium germanate glasses is viewed in terms of a disordered interconnected niobate germanate network, in which NbO_6 units tend to cluster with increasing niobium contents [6]. However, the distribution and local environment of niobium in these glasses has not yet been studied in detail and remains ill-understood. The situation is aggravated by the limited sensitivity of vibrational and nuclear magnetic resonance spectroscopies for detecting structural changes, which in part arises from the limited informational content hitherto obtained from these techniques. While the nuclear isotope ^{93}Nb is 100% naturally abundant and features a moderately sized magnetic moment its suitability for structural applications has been limited by the strong interaction of its nuclear electric quadrupole moment with local electric field gradients,

producing line broadening effects limiting the spectroscopic resolution between different local environments. This feature has posed significant challenges towards the development of more advanced NMR methodology in this area.

Herein, we report the synthesis and structural characterization of optical glasses and glass-ceramics in the system (89.9-*x*)GeO_2-*x*Nb_2O_5-10K_2O-0.1Eu_2O_3, their luminescent properties, and their suitability for micromanufacturing to produce waveguides. The niobium local structure of the glasses and glass-ceramics under study is characterized by solid-state very fast ^{93}Nb MAS and 3QMAS NMR, while the role of the luminescent europium probes is studied by photoluminescence spectroscopy. Finally, 3D waveguide inscription by femtosecond laser irradiation in this material is demonstrated, showing potential for further studies.

2. Experimental part

Eu^{3+}-doped glasses in the system (89.9-*x*)GeO_2-*x*Nb_2O_5-10K_2O-0.1Eu_2O_3 with $x = 0$, 5, 10, 15, and 20 were synthesized using conventional melt-quenching. The samples were labeled *x*Nb, with *x* according to the molar compositions described above. A batch of 10 g of raw materials was homogenized in a mortar, melted in a platinum crucible under ambient conditions at 1500 °C for 1 h, and then cast into a pre-heated stainless-steel mold. Subsequently, the bulk samples were annealed at 500 °C for 4 h to release internal mechanical stress, which resulted from thermal gradients upon cooling. Lastly, glass ceramics were produced from the 15Nb and 20Nb samples by subjecting them to the following heat treatment: 24 h at the first crystallization peak (701 °C) Tc_1, and for separate samples, 24 h at the second crystallization peak T_{C2}.

The characteristic temperatures were obtained from DSC measurements (Figure S1 in the supplementary information), carried out on a Netzsch DSC 404 F3 Pegasus system in the temperature range of 200 to 1200 °C, under a flow of N_2 gas at 50 cm^3 min^{-1} and with a heating rate of 10 °C min^{-1}. Raman spectra were collected using a Jobin-Yvon Horiba-HR800 spectrometer, operating with a He-Ne laser at 632.8 nm.

All ^{93}Nb solid-state nuclear magnetic resonance (NMR) experiments were carried out at a magnetic flux density of 14.1 T using a Bruker Avance Neo 600 spectrometer and fast magic-angle spinning (MAS) at a frequency of ν_{MAS} = 60 kHz achieved in a commercial 1.3 mm double-resonance MAS probe. MAS NMR spectra were recorded using a rotor synchronized $t_{90°}$-τ-$t_{180°}$-rec Hahn-echo sequence [11] employing pulses with durations of 0.6 and 1.2 μs respectively at a ^{93}Nb nutation frequency of ν_{rf} = 150 kHz and using a 16-step phase cycle [12]. The interpulse delay τ was set to ten rotor periods (166.6 μs) in order to allow for sufficient acquisition time for recording the whole echo. After Fourier Transformation, the spectra are shown in their magnitude representation and were subjected to a baseline correction using suitable polynomial functions. Lineshapes were fitted based on the assumption of a wide distribution of nuclear electric coupling strengths affecting the NMR lineshape in the limit of second-order perturbation theory, using the implementation of the Czjzek model in the ssNake software [13]. ^{93}Nb 3QMAS NMR experiments were recorded under the same conditions as the MAS NMR experiments with a three-pulse z-filtered pulse-sequence [14] and 24-step nested phase cycling. The durations of the 3Q excitation, 3Q reconversion, and 1Q conversion pulses were 3.3, 0.6, and 8 μs, respectively, while the rf-amplitude profiles of the first and third pulse (3Q excitation and 1Q conversion) were set according to a WURST pulse with shape parameter N = 2, effectively increasing the 3Q excitation yield and reducing coil ringing upon signal acquisition [14]. 32 consecutive experiments were recorded in the STATES procedure with 6000 scans each, and the delay

between the first two rf-pulses was incremented in steps of $\nu_{MAS}/4$, corresponding to a spectral width of 240 kHz in the indirect dimension. The 3QMAS spectra are shown after appropriate Fourier and shearing transformations. Average values of isotropic chemical shift $<\delta_{iso}>$ and second-order quadrupolar effect, P_Q, are obtained from the center of gravity of the peaks in the anisotropic δ_{D2} and isotropic δ_{D1} projections of the sheared 3QMAS spectra via the following equations,

$$\delta_{\mathrm{iso}} = \frac{17\delta_{D1}+10\delta_{D2}}{27}, \quad (1)$$

$$P_{\mathrm{Q}} = \sqrt{z \cdot 10^{-6}\nu_0^2\,(\delta_{D1} - \delta_{D2})} = C_{\mathrm{Q}}\sqrt{1+\frac{\eta^2}{3}}\ , \quad (2)$$

with $z \approx 453.333$ for $I = 9/2$ and where ν_0, C_Q, and η are the transmitter frequency, the quadrupolar coupling constant, and the asymmetry parameter, respectively.

The photoluminescence (PL) spectra and the PL decay curves were measured at 77 K on a Jobin Yvon Fluorolog spectrofluorimeter, using continuous and pulsed xenon lamps, respectively. Waveguides were written on $69.9GeO_2$-$20Nb_2O_5$-$10K_2O$-$0.1Eu_2O_3$ glass using a femtosecond laser system (Yb:KGW) delivering 216 fs, centered at 1030 nm and operating at a repetition rate of 1 MHz. Femtosecond laser pulses were focused by a 40x objective lens with numerical aperture NA = 0.65. The sample is positioned in a xyz translation stage moved at 30 μm/s perpendicularly to the laser beam. The waveguides were written 100 μm beneath the sample's surface, with laser pulse energy of 90 nJ. The objective-lens-based coupling system was used as described in Ref. [15] to obtain the guiding properties: near-field output profile and optical losses (couple light at 6328 nm). The guided modes were observed with the aid of a CCD camera. The total losses were determined as $L = -10\log(\frac{P_2}{P_1})$, where P_2 represents the output power outgoing from the end facet and P_1 the total input power coming into the waveguide [16].

3. Results and discussion

It is known that binary GeO_2-Nb_2O_5 glasses spontaneously devitrify upon melt-quenching under laboratory conditions resulting in glass-ceramics [17]. The addition of 10 mol% of K_2O increases the Nb_2O_5 solubility in the GeO_2-Nb_2O_5-K_2O system up to 20 mol%, while the doping of such glasses with 0.2 mol% of europium ions does not change significantly the characteristic temperatures and glass structure (see DSC and Raman data in Figures S1 and S2 of the supplementary information, respectively). A previous study [6] suggests that the addition of niobium oxide to germanate glasses progressively occurs under formation of interconnected GeO_y-NbO_x units while further increasing the Nb/Ge ratio results in clustering of NbO_x polyhedra, ultimately leading to crystallization of the glass, forming the phases $K_2Nb_8O_{21}$ and $K_2Nb_{14}O_{36}$.

Figures S3 and S4 of the supplementary information section show the MAS NMR spectra of the glasses, glass-ceramics, and of Nb_2O_5, including both the central (CT) m =1/2 ↔ m = -1/2 and part of the outer Zeeman transitions, which present a wide spinning sideband pattern due to the effect of MAS upon the inhomogeneously broadened lineshapes. The central-transition (CT) MAS NMR spectra (see Figure 1) are dominated by strong quadrupolar interactions affecting the Zeeman frequencies in a manner as predicted by second-order perturbation theory in the presence of a wide distribution of quadrupolar coupling strengths as arising from the structural disorder in the glassy state. This results in asymmetrically broadened, relatively featureless resonance lines, which were modelled by the Czjzek distribution as implemented in the ssNake software [13]. Average chemical shift values are found within the range of -900 to -1300 ppm [18], which is comparable to values measured for ^{93}Nb in niobium silicate [19], tellurite [20,21], phosphate [22-24], and alumino-phosphate glasses [25] and generally attributed to niobium in six-coordination.

Furthermore, the surprisingly poor resolution observed in the spectrum of crystalline Nb_2O_5 needs to be pointed out. The structure of this compound is characterized by a very large number of nonequivalent Nb sites with varying coordination symmetries where the Nb(V) ions are located slightly off-center inside their six-fold coordination polyhedra [21], and are engaged in both corner- and edge-sharing [26,27]. Despite its overall crystalline character, Nb_2O_5 thus features a multitude of local environments that are not well-resolved individually due to anisotropy of the quadrupolar perturbations affecting them, and thus, only a broad asymmetric spectral envelope is observed.

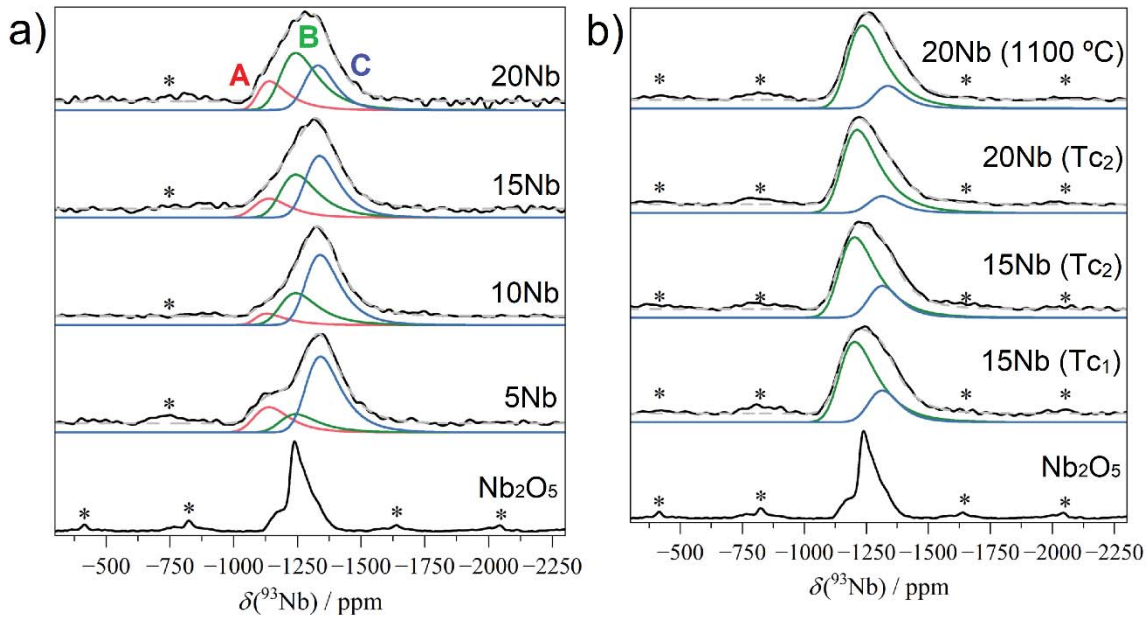

Figure 1: ^{93}Nb CT MAS NMR spectra (black lines) of (89.9-*x*)GeO_2-*x*Nb_2O_5-10K_2O-0.1Eu_2O_3 of the (a) glasses and (b) glass-ceramics and Nb_2O_5. Asterisks indicate spinning-sidebands which can be differentiated from the noise. Blue, green, and red lines are simulated lineshapes according to the Czjzek distribution model, while the dashed gray line is the sum of fits.

The main peak found in the spectra of the glasses is found at an isotropic chemical shift of about -1280 ppm, while for a Nb_2O_5 content of 20% the component near -1180 ppm becomes dominant. The heat treatments of the glasses produce significant changes in the spectra of the glass-ceramics, i.e., low-frequency shifts of the center-of-gravity, but the spectra of the glass-ceramics show no improved resolution or new distinct spectral features despite the formation of $K_2Nb_{14}O_{36}$ and $K_2Nb_8O_{21}$ bronze-like perovskites [6]. Rather, broad signals can be observed at an isotropic chemical shift of -1150 ppm, coinciding with the center-of-gravity of the Nb_2O_5 spectrum. No significant difference can be observed between the spectra measured on the samples crystallized at T_{c1} ($K_2Nb_{14}O_{36}$) and those crystallized at T_{c2} ($K_2Nb_8O_{21}$). It is known that for crystalline Nb-containing compounds where corner- or edge-sharing occurs exclusively between two Nb polyhedra, i.e., in octahedral $[Nb(ONb)_6]$ units, the chemical shifts are closer to -1000 ppm while the presence of more electronegative elements X in the second-coordination sphere, as in $[Nb(OX)_{6-y}(ONb)_y]$ units (with $1 \leq y \leq 5$), results in a shift towards lower frequencies, e.g., from -1300 to -1650 ppm (center of gravity) for X = P [24]. The same effect on the chemical shift is conceivable for the Nb species in the glasses and glass-ceramics of the present study, given that Ge possesses a similar electronegativity and atomic radius compared to P. Thus, for the glasses, we attribute the main peak of the ^{93}Nb MAS NMR spectra at -1280 ppm to $[Nb(OGe)_{6-y}(ONb)_y]$ structural units with a rather low y value reaching down to isolated $[Nb(OGe)_6]$ units (site C), while for the glass-ceramics, the main peak near -1150 ppm is attributed to $[Nb(OGe)_{6-y}(ONb)_y]$ structural units with high y values up to $[Nb(ONb)_6]$ units (site B). Interestingly, with increasing Nb content the intensity of the main peak in the glasses (site A) decreases monotonically, while the intensity of the high-frequency shoulder first decreases, then increases again beyond 10% Nb_2O_5 while moving to slightly lower frequencies near -1090 ppm. These changes likely indicate conversions between different $[Nb(OGe)_{6-y}(ONb)_y]$

units, towards the situation in the glass-ceramics. In fact, it was observed in niobium phosphate glasses and in preliminary data on Li_2O-Nb_2O_5-SiO_2 glasses, that for higher Nb contents a non-intermixed niobate network forms at the expense of the intermixed network [23-25].

To better understand and document the spectral changes of the glasses and glass-ceramics, ^{93}Nb 3QMAS NMR experiments were performed on selected samples. All δ_{iso} and P_Q values, extracted from the 3QMAS NMR spectra are listed in Table 1. In general, despite using a high sampling rate for the evolution of the 3Q intensity (i.e., using a short increment for the first interpulse delay of 4.17 μs) only few increments with signal were obtained even in the high Nb-containing samples, e.g., 16 for the 20Nb glass sample and about 32 for Nb_2O_5, leading to limited resolution and signal-to-noise ratios. For the glasses (see Figure 2 left), all spectra reproduce well the main peak visible in the MAS NMR spectra near -1280 ppm, however, principally in the spectra of samples 5Nb and 15Nb, as well as for Nb_2O_5, the high frequency shoulder is missing. Upon closer inspection, it can be seen that the vertical projections of the 3QMAS NMR spectra of the latter samples (top and center-left) confirm the presence of a peak near -1050 ppm, however, with much decreased intensity. Such an underrepresentation in the 3QMAS NMR spectrum may arise either due to a reduced 3Q excitation efficiency, affecting ^{93}Nb nuclei subjected to significantly stronger quadrupolar coupling (larger C_Q values), or a much shorter transversal relaxation time T_2 for certain ^{93}Nb nuclei, promoted by the chemical environment of the Nb site. In fact, we found such reduced T_2 values in a series of Li_2O-Nb_2O_5-SiO_2 glasses and it was reported elsewhere that for a series of high alkali-ion containing Nb-based glasses the acquisition of 3QMAS NMR was entirely impossible [25]. On the other hand, given the peak position of the high frequency component of glass 5Nb, i.e., -1133 and -1054 ppm in the anisotropic and isotropic dimensions respectively, a P_Q value of about 28 MHz can be extracted from the

3QMAS spectrum according to Eq. 2 and an isotropic chemical shift of δ_{iso} = -1083 ppm. This former value is of comparable size to those of the other two signal components of about 27.1 MHz (δ_{iso} = -1191 ppm) and 27.6 MHz (δ_{iso} = -1296 ppm), thus comparable 3Q excitation efficiency for all components are expected. For the above reasons we attribute the shoulder near -1100 ppm (d_{iso} = 1080 ppm) to Nb species within $[Nb(OGe)_{6-y}(ONb)_y]$ structural units with rather high y values between 4 and 6, that possibly bear non-bridging oxygen atoms charged compensated by K^+ ions (site A). For the glass-ceramics (see Figure 2 right) the 3QMAS NMR data reveals no additional lineshape features or narrow peaks and signal intensity near -1100 ppm is absent altogether. However, for all samples significant intensity is missing towards the low frequency shoulder of the spectra, likely owed to a reduced 3Q excitation efficiency for those Nb nuclei subjected to very large C_Q values within the given distribution of quadrupolar parameters.

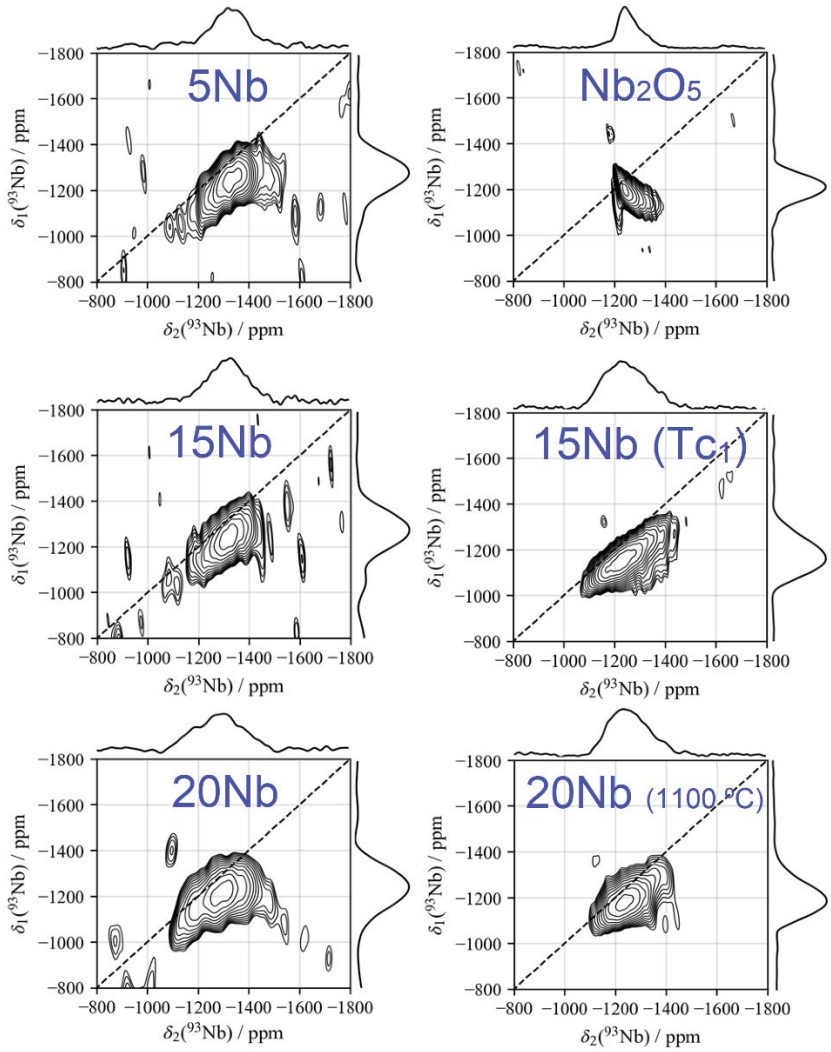

Figure 2: ^{93}Nb TQMAS NMR spectra of (89.9-x)GeO_2-$x$$Nb_2O_5-10K_2O-0.1Eu_2O_3$ glasses (left) and glass-ceramics, as well as Nb_2O_5 (right). The dashed diagonal lines indicate the isotropic dimension.

Based on the spectral editing provided by Figure S5 and after careful analysis, successful deconvolutions of the MAS NMR spectra were achieved by simulations employing three signal components according to Czjzek distributions of the quadrupolar NMR parameters. The deconvolution result is depicted as red, green, and blue lines in Figures 1.a and 1.b, and the extracted NMR parameters are listed in Table 1. The extracted mean quadrupolar coupling constants, $\overline{C_Q}$, are found in good agreement with the P_Q values

from the 3QMAS NMR spectra. It was found that simulating the glass spectra with only two signal components could not account for the signal intensity near -1250 ppm, coinciding with the observed peak maxima of Nb_2O_5 and the glass-ceramics. Thus, we attribute the blue and red lines to sites C and A, accordingly to the above discussions to the peaks near -1300 and -1100 ppm respectively, while the green line (site B) represents NbO_6 species within $[Nb(OGe)_{6-y}(ONb)_y]$ structural units whose second coordination-sphere is dominated by other Nb atoms, i.e., with rather high *y* values. It is worthwhile noting that for the 20Nb glass this latter signal component strongly dominates the spectrum, indicating its structural similarity to their glass-ceramics caused by clustering of $[Nb(ONb)_6]$ units. Furthermore, for the glass-ceramics, it was not possible to simulate the spectra with a single Czjzek distribution of quadrupolar parameters. In agreement with the observed shoulder in the 3QMAS spectra of the glass-ceramics near -1300 ppm (Figure 2), we have therefore considered a second signal component, attributable to intermixed Nb-O-Ge linkages found in the residual glass. Given the above results, the data suggest that for increasing Nb contents in $(89.9-x)GeO_2$-xNb_2O_5-$10K_2O$-$0.1Eu_2O_3$ glasses the local structure becomes increasingly dominated by $[Nb(ONb)_6]$ units at the expense of intermixed $[Nb(OGe)_{6-y}(ONb)_y]$ structural units. Lastly, the crystallization of the glasses during heat treatment appears to have a similar effect, converting $[Nb(OGe)_{6-y}(ONb)_y]$ structural units with low *y* values, and those requiring charge compensation by K^+, to such units with high *y* values up to $[Nb(ONb)_6]$, while some residual glass remains.

The luminescent features of Eu^{3+} ions were studied to probe the rare-earth local environment, which is paramount for rare-earth photoluminescence efficiency and photonic applications. Photoluminescence excitation (PLE) spectra for the glass samples under study and glass-ceramic samples with 20mol% are shown in Figure 3.a. The absorption spectra display characteristic f-f transitions of Eu^{3+} ions from the ground state $^7F_0$ to the excited

levels $^5D_4$ (361 nm), $^5G_2$ (381 nm), $^5L_6$ (393 nm), $^5D_3$ (413 nm), $^5D_2$ (464 nm), and $^5D_1$ (531 nm). It can be observed that the PLE profile is dependent on the glass composition and degree of glass crystallization. A progressive spectral broadening is visible upon increasing the niobium content owed to the increase of niobate-germanate unit cross-linking, in agreement with the ^{93}Nb NMR data. This modification consequently leads to a greater distribution of suitable host sites for the RE ions, i.e., Eu^{3+} will be situated within sites with greater differences in metal-ligand angles and distances, such as near $[Nb(OGe)_{6-y}(ONb)_y]$ units with $1 \leq y \leq 5$. Furthermore, a greater spectral change is observable upon glass-ceramics formation suggesting a modification in the Eu^{3+} chemical environment, possibly due to an increase of local ordering. In this perspective, the phonon sideband (PSB) was investigated as it provides additional information about vibration modes and the local environment of the Eu^{3+} ions [28]. The PSB matches up to the $^7F_0 \rightarrow {}^5D_2$ transition (Figure 3.b) and is the difference the between energy of zero phonon line (ZPL) at 464 nm (21552 cm^{-1}) to phonon line identified around 450 and 445 nm (22182 and 22452 cm^{-1}). These vibrational modes are ascribed to the Nb-O and Ge-O units, respectively. A PSB redshift occurs with niobium insertion into glass due to a lower resulting phonon energy in the Ge-O-(Nb) environment. Regarding the effect of the thermal heat treatments, the appearance of PSB attributed to Nb-O vibrational modes was identified after the glass-ceramic formation and suggests the presence of RE ions in proximity to crystalline niobium oxide domains, i.e., within $[Nb(OGe)_{6-y}(ONb)_y]$ units with rather high y values priorly attributed to site B.

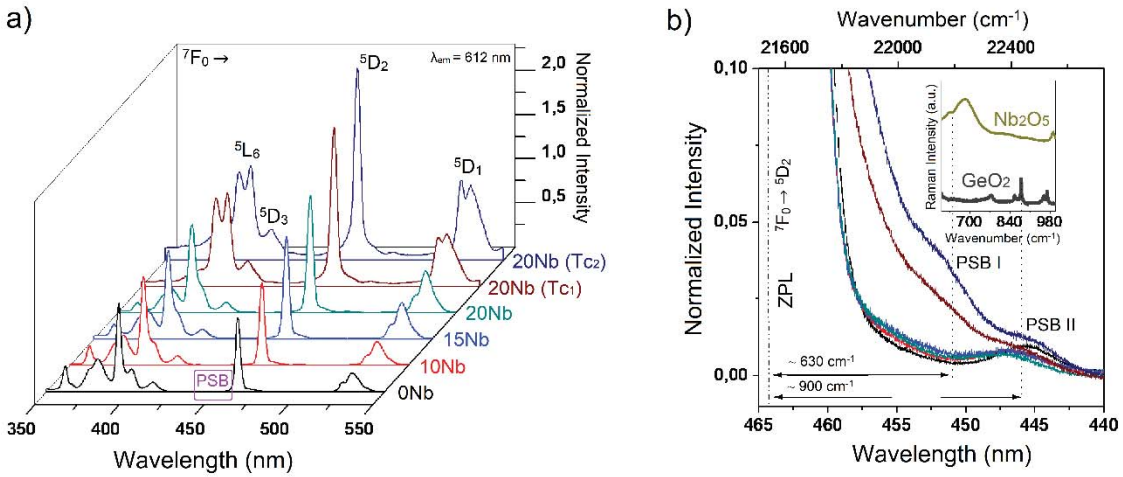

Figure 3. (a) PLE spectra (normalized at 464 nm) and (b) phonon sidebands of the glasses and glass-ceramics.

The photoluminescence (PL) emission spectra for the glasses and glass-ceramics are shown in Figures 4 and 5, respectively. Emission bands at 580, 595, 612, 656, and 704 nm are observable originating from Eu^{3+} transitions going out from the metastable $^5D_0$ state to different lower energy states, i.e., ^7F_J (J = 0, 1, 2, 3 and 4). Judd-Ofelt radiative parameters of the Eu^{3+}-doped glasses were calculated from the $^5D_0 \rightarrow {}^7F_1$ transition, which is only allowed via a magnetic dipole, allowing other transitions to be derived from their intensity [29]. Some significant changes can be seen in the glasses upon niobium insertion: (1) a reduction of the $^5D_0 \rightarrow {}^7F_0/{}^7F_1$ ratio; (2) a reduction of the $^5D_0 \rightarrow {}^7F_2/{}^7F_1$ ratio; (3) a lowered Ω_2 parameter and (4) shorter luminescence lifetimes. Specifically, the J = 0 → J' = 0 ($^5D_0 \rightarrow {}^7F_0$ transitions) are forbidden according to Judd–Ofelt theory, however, they may appear in low symmetries (C_n, C_{nv}, C_s) due to J-mixing in the presence of certain crystal field perturbations [30]. In this perspective, the decrease in the relative intensity of this emission also points towards an increase in the local symmetry of Eu^{3+} ions, further corroborated by the decrease in $^5D_0 \rightarrow {}^7F_2$ hypersensitive transition intensity. The $^5D_0 \rightarrow {}^7F_1$ and $^5D_0 \rightarrow {}^7F_2$ transitions occur via magnetic (relatively insensitive to the local symmetry) and electric

dipole couplings, respectively. The $^5D_0 \rightarrow {}^7F_2$ transition is hypersensitive to changes in the Eu^{3+} coordination geometry and tends to be more intense in asymmetric sites [30]. Therefore, the lowered $^5D_0 \rightarrow {}^7F_2/{}^5D_0 \rightarrow {}^7F_1$ ratio indicates the preferential occupation of Eu^{3+} ions in higher symmetry sites with niobium content. Likewise, the Ω_2 parameter, which is usually related to the covalence of the RE-O bonds [31] and angular changes in the local coordination geometry of the RE [32], shows that the covalence character of the Eu-O bonds decreases as expected for an increasingly Nb rich environment [33] and ultimately approaches that reported for niobium silicate nanostructured materials ($\Omega_2 = 1.04 \times 10^{-19}$ cm^2 for Nb/Si ratio = 0.7) [34]. Finally, the experimental Eu^{3+} $^5D_0$ lifetime values for 0Nb, 10Nb, 15Nb and 20Nb were measured as 1.92, 1.44, 1.46, 1.31 ms, respectively. The lifetime decreases after niobium addition due to the increased local refractive index close to Nb-O bonds, corroborating the results drawn from the analysis of the Ω_2 parameter and PSB analysis. To summarize, the set of these interpretations unanimously demonstrates that the symmetry of the first coordination shell of Eu^{3+} ions increases with niobium content. This can be explained by the preferential accommodation of Eu^{3+} ions in proximity to the still amorphous but niobium polyhedra-rich environment (site B in the ^{93}Nb NMR data) as illustrated in Figure 4.

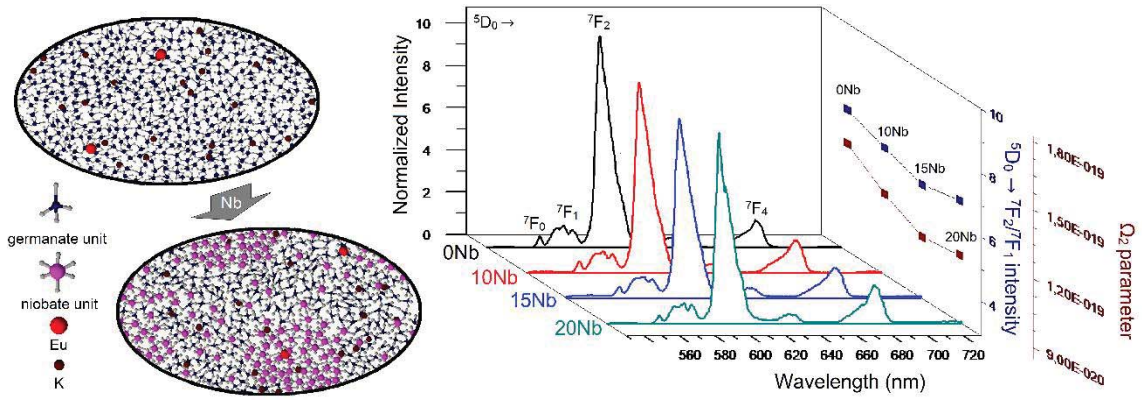

Figure 4. PL spectra of the glasses upon excitation at 464 nm (normalized to the maximum intensity of the band near 595 nm) and structure illustration of Eu^{3+}-doped alkali germanate glass (0Nb, top structure) and Eu^{3+}-doped alkali niobium germanate glass (20Nb, bottom structure). The PL decay curves of $^5D_0$ excited state as shown in the inset of Figure 2.

PL spectra for the glass-ceramics (see Figure 5) were collected after heat treatment for 15 min in steps of 10 °C along with the temperature range of 590-860 ºC. These spectra show the continuous decrease of the $^5D_0 \rightarrow {}^7F_0/{}^7F_1$ and $^5D_0 \rightarrow {}^7F_2/{}^7F_1$ ratios as well as the Ω_2 parameter. Thus, similar to the situation of the glasses, the Eu^{3+} ions appear to be increasingly incorporated into more symmetrical and niobium-rich environments, concomitantly to the crystallization process. Interestingly, the split of the band corresponding to $^5D_0 \rightarrow {}^7F_J$ transitions suggests the crystallization modifies the crystal-field strengths around Eu^{3+} ions resulting in an increased resolution of the Stark components of the emission multiplet, in accordance with the PSB data.

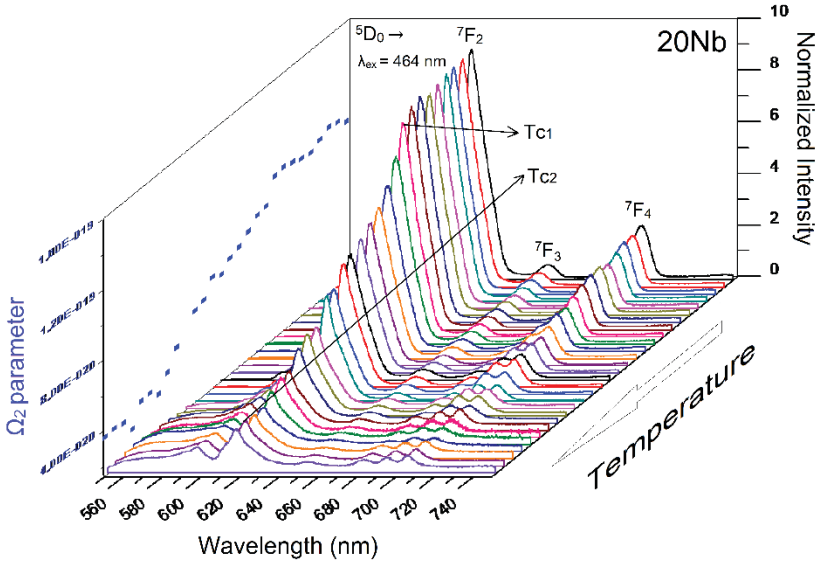

Figure 5. PL spectra upon excitation at 464 nm of the glass-ceramics at different heat treatment temperatures (590-860 ºC increasing from 10 to 10 ºC). For clarity, each curve is normalized in 595 nm.

Finally, we demonstrate the fabrication of waveguides, by fs-laser micromachining on the bulk of a glass sample containing 20mol% of Nb_2O_5. Figure 6a shows optical microscopy images of the cross-section (a) and top (b) view of a typical waveguide fabricated, written 100 µm below the surface. The images unveil the waveguides are homogeneous along their entire length, with a cross-section of approximately 2 µm. Figure 6.c shows the near-field output profile of the light guided at 632.8 nm. The waveguides presented total losses (coupling and propagation) inferior to 0.6 ± 0.2 dB/mm at 632.8 nm.

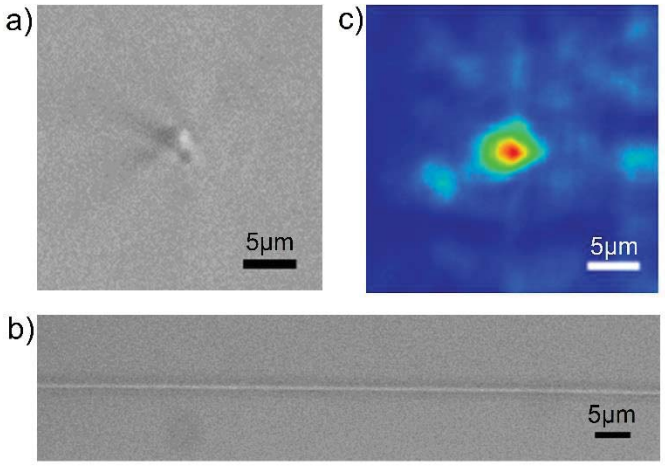

Figure 6. (a) Cross-section and (b) top-view optical microscopy images of the waveguides in 20Nb glass fabricated by femtosecond pulse (260 fs, 1 MHz, 90 nJ); and (c) near-field output profile of the light guided at 632.8 nm.

Thus, this paper described a combined structural and luminescence (structural probe) study in niobium germanate glass and glass-ceramics. The results point to the great potential of the material for photonic applications. NbO_6-rich regions are hosts of rare-earth ions causing a clear luminescent properties modification, and the precipitated perovskite bronze-like structure in the glass-ceramic is of interest for linear and nonlinear optical applications. The successful fabrication of waveguides in the material volume highlights the potential for applications in photonic microdevices.

4. Conclusion

Eu^{3+}-doped alkali niobium germanate glasses and glass-ceramics were synthesized and the local structure of niobium and the rare-earth ions was investigated by nuclear magnetic resonance and luminescence spectroscopy. For the first time, deconvolutions of the ^{93}Nb MAS NMR spectra into individual sites were achieved employing three signal

components according to Czjzek distributions of the quadrupolar NMR parameters. The attribution of the fit components to three distinct Nb environments was corroborated by the distinct spin-dynamics revealed by 3QMAS NMR spectroscopy: niobium species within $Nb(OGe)_{6-y}(ONb)_y$ polyhedra comprising low *y*-values, high *y*-values, and high *y*-values bearing non-bridging oxygen atoms charge compensated by K^+ ions.

Based on photoluminescence spectroscopy it could be demonstrated that the chemical environment of the sensitive Eu^{3+} ions is dominated by $Nb(OGe)_{6-y}(ONb)_y$ polyhedra with rather high *y*-values for glasses with high Nb content and glass-ceramics. This selective occupation of niobium-rich domains is favorable for the development of all-optical communication devices due to low local phonon energy and reduced nonradiative processes. A preliminary investigation showed the feasibility of producing 3D waveguides by using femtosecond lasers proving their potential for all-optical communication systems and switches.

Acknowledgments

The authors would like to thank Brazilian funding agencies CNPq (Project N. 156420/2018-0), CAPES for financial support and further FAPESP (grant 2013/07793-6, CeRTEV-CEPID program) for the lab facilities. LM is grateful for support from the São Paulo Research Foundation (FAPESP) with grant number 2020/01786-1. HB is grateful for support from the São Paulo Research Foundation (FAPESP) with grant number 2019/26399-3.

References

[1] Xu, K.; Zhang, B. Y.; Hu, Y.; Khan, M. W.; Ou, R.; Ma, Q.; Shangguan, C.; Murdoch, B. J.; Chen, W.; Wen, X.; Ren, G.; Ou J. Z. A high-performance visible-light-driven all-optical switch enabled by ultra-thin gallium sulfide, J. Mater. Chem. C. 9 (2021) 3115-3121. DOI: 10.1039/D0TC05676F

[2] Chen, H.; Wang, C.; Song, Y.; Tian, J. All-optical modulation with 2D layered materials: status and prospects, Nanophotonics 9:8 (2020) 2107-2124. DOI: 10.1515/nanoph-2019-0493

[3] Bai, J.; Long, X.; Liu, C. Ridge waveguides in Yb^{3+}-doped silicate glass fabricated by combination of proton implantation and femtosecond laser ablation, Mater. Res. Express 7 (2020) 105201. DOI: 10.1088/2053-1591/abc219

[4] Liu, C-X.; Li, Y-W.; Fu, L-L.; Zhang L-L.; Guo, H-T.; Zhou, Z-G.; Li, W-N.; Lin, S-B.; Wei W. Optical waveguides in magneto-optical glasses fabricated by proton implantation, Opt. Laser Technol. 85 (2016) 55-59. DOI: 10.1016/j.optlastec.2016.05.008

[5] Lai, C-C.; Lo, C-Y.; Huang, J-Z.; Chiang, C-C. F.; Nguyen, D. H.; Chen, Y-P.; Liao, C-D. Architecting a nonlinear hybrid crystal–glass metamaterial fiber for all-optical photonic integration, J. Mater. Chem. C 6 (2018) 1659-1669. DOI: 10.1039/C7TC05112C

[6] Marcondes, L.M.; Maestri, S.; Souza, B.; Gonçalvez, R. R.; Cassanjes, F. C.; Poirier, G. Y.; High niobium oxide content in germanate glasses: Thermal, structural, and optical properties, J. Am. Ceram. Soc. 101 (2018) 220-230. DOI: 10.1111/jace.15215

[7] Manzani, D.; Gualberto, T.; Almeida, J. M. P.; Montesso, M.; Mendonça, C. R.; Rivera, V. A. G.; Boni, L. Nalin, M.; Ribeiro, S. J. L.; Highly nonlinear Pb2P2O7-Nb2O5 glasses for optical fiber production, J. Non-Cryst. Solids 443 (2016) 82-90. DOI: 10.1016/j.jnoncrysol.2016.04.019

[8] Lippincott, E. R.; Valkenburg, a. v.; Weir, C. E.; Bunting, E. N. Infrared Studies on Polymorphs of Silicon Di oxide and Germanium Dioxide J. Res. Natl. Bur. Stand. 61:1 (1958) 61-70. DOI: 10. 10.6028/jres.061.009

[9] Marcondes, L. M.; Rodrigues, L.; Cunha, C. R. da; Gonçalves, R. R.; Camargo, A. S. S. de; Cassanjes, F. C.; Poirier, G. Y. Rare-earth ion doped niobium germanate glasses and glass-ceramics for optical device applications. J. Lumin. 213 (2019) 224-434. DOI: 10.1016/j.jlumin.2019.05.012

[10] Marcondes, L. M.; Evangelista, R. O.; Gonçalves, R. R.; A. S. S. de Camargo, A. S. S. de; Manzani, D.; Nalin, M.; Cassanjes, F. C.; Poirier, G. Y. Er^{3+}-doped niobium alkali germanate glasses and glass-ceramics: NIR and visible luminescence properties. J. Non-Cryst. Solids 521 (2019) 119492. DOI: 10.1016/j.jnoncrysol.2019.119492

[11] Hahn, E. L. Spin Echoes, Phys. Rev. 80:4 (1950) 580-594. DOI: 10.1103/PhysRev.80.580

[12] Kunwar, A. C.; Turner, G.; Oldfield E. Solid-state spin-echo Fourier transform NMR of ^{39}K and ^{67}Zn salts at high field, J. Magn. Reson. 69:1 (1986) 124-127. DOI: 10.1016/0022-2364(86)90224-6

[13] Meerten S. G. J.; Franssen W. M. J.; Kentgens, A. P. M. ssNaKe: A cross-plaform open-source NMR data processing and fitting application, J. Magn. Reson. 301 (2019) 56-66. DOI: 10.1016/j.jmr.2019.02.006

[14] Koppe, J.; Knitsch, R.; Wegner, S.; Hansen, M. R. Sensitivity-enhanced multiple-quantum MAS NMR for half-integer spin quadrupolar nuclei using WURST-amplitude shaped pulses, J. Magn. Reson. 321 (2020) 106873. DOI: 10.1016/j.jmr.2020.106873

[15] Almeida, J. M. P.; Ferreira, P. H. D.; Manzani, D.; Napoli, M.; Ribeiro, S. J. L.; Mendonça, C. R. Metallic nanoparticles grown in the core of femtosecond laser micromachined waveguides, J. Appl. Phys. 115 (2014) 193507. DOI: 10.1063/1.4875485

[16] Babu, B. H.; Niu, M.; Yang, X.; Wang, Y.; Feng, L.; Qin W.; Hao, X-T. Systematic control of optical features in aluminosilicate glass waveguides using direct femtosecond laser writing, Opt. Mater. 72 (2017) 501-507. DOI: 10.1016/j.optmat.2017.06.049

[17] Levin, E. M. Equilibria in the System Niobium Pentoxide Germanium Dioxide, J. Res. Nat. Bur. Stand - Section A. 70:1 (1966) 5-10. DOI: 10.6028/jres.070A.002

[18] Lapina, O B.; Khabibulin, D. F.; Romanenko, K. V.; Gan, A.; Zuev, M. G.; Krasilnikov, N.; Fedorov, V. E. ^{93}Nb NMR chemical shift scale for niobia systems, Solid State Nucl. Magn. Reson. 28:2-4 (2005) 204-224. DOI: 10.1016/j.ssnmr.2005.09.003

[19] Drake, K. O.; Carta, D.; Skipper, L. J.; Sowrey, F. E.; Newport, R. J.; Smith, M. E. A multinuclear solid state NMR study of the sol-gel formation of amorphous Nb_2O_5-SiO_2 materials, Solid State Nucl. Magn. Reson. 27:1-2 (2005) 28-36. DOI: 10.1016/j.ssnmr.2004.08.008

[20] Dolhen, M.; Allix, M.; Sarou-Kanian,V.; Fayon, F.; Genevois, C.; Chenu, S.; Coulon, P-E.; Colas, M.; Cornette, J.; Duclère, J-R.; Brisset, F.; Masson, O.; Thomas, P.; Delaizir, G. A comprehensive study of the glass/translucent anti-glass/transparent ceramic structural ordering in the $Bi_2O_3Nb_2O_5TeO_2$ system, Acta Mater. 189 (2020) 73-84. DOI: 10.1016/j.actamat.2020.02.062

[21] Hart, R. T.; Anspach, M. A.; Kraft, B. J.; Zaleski, J. M.; Zwanziger, J. W.; DeSanto, P J.; Stein, B.; Jacob, J.; Thiyagarajan. Optical Implications of Crystallite Symmetry and Structure in Potassium Niobate Tellurite Glass Ceramics, Chem. Mater. 14:10 (2002) 4422–4429. DOI: 10.1021/cm020615q

[22] Kalenda, P.; Koudelka, L.; Mosner, P.; Montagne, L.; Revel, B.; Trebosc, J. Glass to crystal transformation in the ternary BaO-Nb_2O_5-P_2O_5 system, J. Mol. Struct. 1143 (2017) 472-477. DOI: 10.1016/j.molstruc.2017.04.112

[23] Flambard, A.; Montagne, L.; Delevoye, L.; Palavit, G.; Amoureux, J-P.; Videau, J-J. Solid-state NMR study of mixed network sodium–niobium phosphate glasses, J. Non-Cryst. Solids 345-346 (2004) 75-79. DOI: 10.1016/j.jnoncrysol.2004.07.046

[24] Flambard, A.; Videau, J-J.; Delevoye, L.; Cardinal. T.; Labrugère, C.; Rivero, C. A.; Couzi, M.; Montagne, L. Structure and nonlinear optical properties of sodium–niobium phosphate glasses, J. Non-Cryst. Solids 354 (2008) 3540-3547. DOI: 10.1016/j.jnoncrysol.2008.03.017

[25] Chenu, S.; Werner-Zwanziger, U.; Calahoo, C.; Zwanziger, J. W. Structure and properties of $NaPO_3$-ZnO-Nb_2O_5-Al_2O_3 glasses, J. Non-Cryst. Solids 358 (2012) 1795-1805. DOI: 10.1016/j.jnoncrysol.2012.05.027

[26] Khabibulin, D.; Konstantin, R.; Zuev, M.; Olga, L. Solid state NMR characterization of individual compounds and solid solutions formed in Sc_2O_3-V_2O_5-Nb_2O_5-Ta_2O_5 system, Magn. Reson. Chem. 45:11 (2007) 962-970. DOI: 10.1002/mrc.2086

[27] Flambard, A.; Montagne, L.; Delevoye, L.; Steuernagel, S. ^{93}Nb and ^{17}O NMR chemical shifts of niobiophosphate compounds, Solid State Nucl. Magn. Reson. 32:2 (2007) 34-43. DOI: 10.1016/j.ssnmr.2007.07.001

[28] Polosan, S. Crystallization processes in europium-doped $Bi_4Ge_3O_{12}$ glass materials, J. Lumin. 213 (2019) 235-240. DOI: 10.1016/j.jlumin.2019.05.031

[29] Carlos, L. D.; Ferreira, R. A.; Bermudez, V. Z.; Ribeiro, S. J. Lanthanide-containing light-emitting organic-inorganic hybrids: A bet on the future. Adv. Mater 51 (2009) 509-534. DOI: 10.1002/adma.200801635

[30] Binnemans, K. Interpretation of europium(III) spectra. Coord. Chem. Rev 295 (2017) 1-45. DOI: 10.1016/j.ccr.2015.02.015

[31] R. Reisfeld, R.; Jorgensen, C. K. Excited state phenomena in vitreous materials. In: Handboook on the Physics and Chemistry of Rare Earth, 9:58 (1987).

[32] Silva, I. G. N.; Mustafa, D.; Andreoli, B.; Felinto, M. C. F. C.; Malta, O. L.; Brito, H. F. Highly luminescente Eu^{3+}-doped benzenetricarboxylate bases materials. J. Lumin. 170 (2016) 364-368. DOI: 10.1016/j.jlumin.2015.04.047

[33] Marcondes, L. M.; da Cunha, C. R.; de Sousa, B. P.; Maestri, S.; Gonçalves, R. R.; Cassanjes, F. C.; Poirier, G. Y. Thermal and Spectroscopic properties studies of Er^{3+}-doped and Er^{3+}/Yb^{3+}-codoped niobium germanate glasses for optical applications. J. Lumin. 205 (2018) 487-494. DOI: 10.1016/j.jlumin.2018.09.046

[34] Caixeta, F. J.; Alquino, F. T.; Pereira, R. R.; Gonçalves, R. R. Highly red luminescent $Nb_2O_5:Eu^{3+}$ nanoparticles in silicate host for solid-state lighting and energy conversion. Opt. Mater. 111 (2021) 110671. DOI: 10.1016/j.optmat.2020.110671

Figure Captions

Figure 1: ^{93}Nb CT MAS NMR spectra (black lines) of (89.9-*x*)GeO_2-*x*Nb_2O_5-10K_2O-0.1Eu_2O_3 of the (a) glasses and (b) glass-ceramics and Nb_2O_5. Asterisks indicate spinning-sidebands which can be differentiated from the noise. Blue, green, and red lines are simulated lineshapes according to the Czjzek distribution model, while the dashed gray line is the sum of fits.

Figure 2: ^{93}Nb TQMAS NMR spectra of (89.9-*x*)GeO_2-*x*Nb_2O_5-10K_2O-0.1Eu_2O_3 glasses (left) and glass-ceramics, as well as Nb_2O_5 (right). The dashed diagonal lines indicate the isotropic dimension.

Figure 3. (a) PLE spectra (normalized at 464 nm) and (b) phonon sidebands of the glasses and glass-ceramics.

Figure 4. PL spectra of the glasses upon excitation at 464 nm (normalized to the maximum intensity of the band near 595 nm) and structure illustration of Eu^{3+}-doped alkali germanate glass (0Nb, top structure) and Eu^{3+}-doped alkali niobium germanate glass (20Nb, bottom structure). The PL decay curves of $^5D_0$ excited state as shown in the inset of Figure 2.

Figure 5. PL spectra upon excitation at 464 nm of the glass-ceramics at different heat treatment temperatures (590-860 ºC increasing from 10 to 10 ºC). For clarity, each curve is normalized in 595 nm.

Figure 6. (a) Cross-section and (b) top-view optical microscopy images of the waveguides in 20Nb glass fabricated by femtosecond pulse (260 fs, 1MHz, 90 nJ); and (c) near-field output profile of the light guided at 632.8 nm.

Table 1: ^{93}Nb NMR parameters, isotropic chemical shift (δ_{iso}), average quadrupole coupling constant ($\overline{C_Q}$), (Czjzek) distribution width of quadrupolar coupling constants (σ), quadrupolar product (P_Q), Gaussian line broadening (FWHM GB), FWHM of the chemical shift distribution (ΔCS) and area fraction (f) of the (89.9-x)GeO_2-$x$$Nb_2O_5-10K_2O-0.1Eu_2O_3$ glasses and glass-ceramics extracted from 3QMAS NMR data and obtained by simulation of the MAS NMR spectra using the Czjzek model.

Sample / Site		δ_{iso} / ppm		$\overline{C_Q}$ (σ) / MHz	P_Q / MHz	FWHM GB / kHz	ΔCS / kHz	f / %
		Czjzek ± 5 ppm	3QMAS ± 10 ppm	Czjzek ± 2.5 MHz	3QMAS ± 5 MHz	Czjzek	3QMAS ± 2.5 kHz	MAS ± X %
Nb_2O_5								
			-1208		27.8		8	
			-1124		31.3		6	
Glasses								
5Nb	A	-1080	-1083	31.0 (17.5)	28.0	15.0	8.0	21
	B	-1180	-1191*	33.0 (18.6)	27.1*	15.0	10.0*	16
	C	-1282	-1296	31.0 (17.4)	27.6	15.0	10.0	63
10Nb	A	-1080	-	31.0 (17.5)	-	10.0	-	9
	B	-1180	-	33.0 (18.6)	-	15.0	-	30
	C	-1282	-	30.0 (17.0)	-	15.0	-	61
15Nb	A	-1080	-1083	31.0 (17.5)	27.8	15.0	8.0	15
	B	-1180	-1182*	33.0 (18.6)	28.5*	15.0	10.0*	37
	C	-1282	-1260	30.0 (16.5)	27.4	15.0	12.0	49
20Nb	A	-1090	-1087	31.0 (17.5)	29.0	10.0	8.0	20
	B	-1180	-1184*	33.0 (18.6)	25.4*	15.0	10.0*	49
	C	-1282	-1270	28.0 (15.0)	30.5	15.0	14.0	31
Glass-Ceramics								
15Nb TC_1		-1138	-1177	33.5 (19.0)	28.0	15.0	13	76
		-1263	-1292 – -1242*	28.5 (15.6)	32.1 – 38.2*	15.0	10	24
15Nb TC_2		-1138		33.5 (19.0)		15.0		76
		-1263		28.5 (15.6)		15.0		24
20Nb TC_2		-1148		33.5 (19.0)		15.0		86
		-1263		28.5 (15.6)		15.0		14
20Nb 1100 °C		-1170	-1195	33.3 (18.8)	28.7	15.0	12	82
		-1289	-1297	28.3 (14.9)	23.2	15.0	10	18

*Greater uncertainty

Supporting Information

Structural and Luminescence Characterization of Europium-doped Niobium Germanate Glasses: Novel insights from ^{93}Nb Solid-State NMR Spectroscopy

Lia Mara Marcondes, Henrik Bradtmüller, Sabrina Nicoleti Carvalho dos Santos, Lucas Konaka Nolasco, Cleber Renato Mendonça, Silvia Helena Santagneli, Gael Yves Poirier, Marcelo Nalin

DSC data

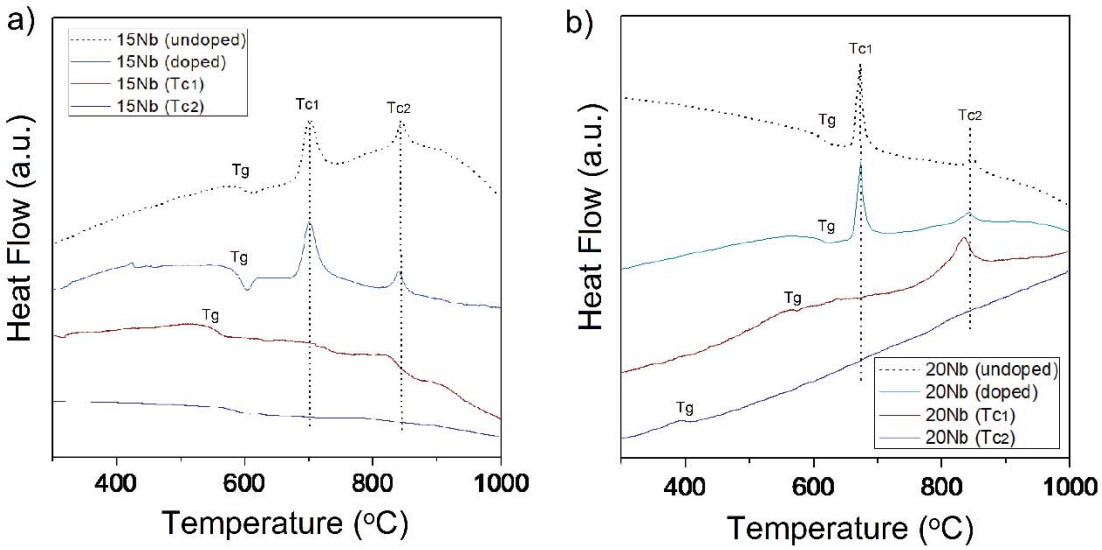

Figure S1. DSC curves of undoped and Eu^{3+}-doped alkali niobium germanate glasses and respective glass-ceramics (a) 15Nb and (b) 20Nb.

Raman data

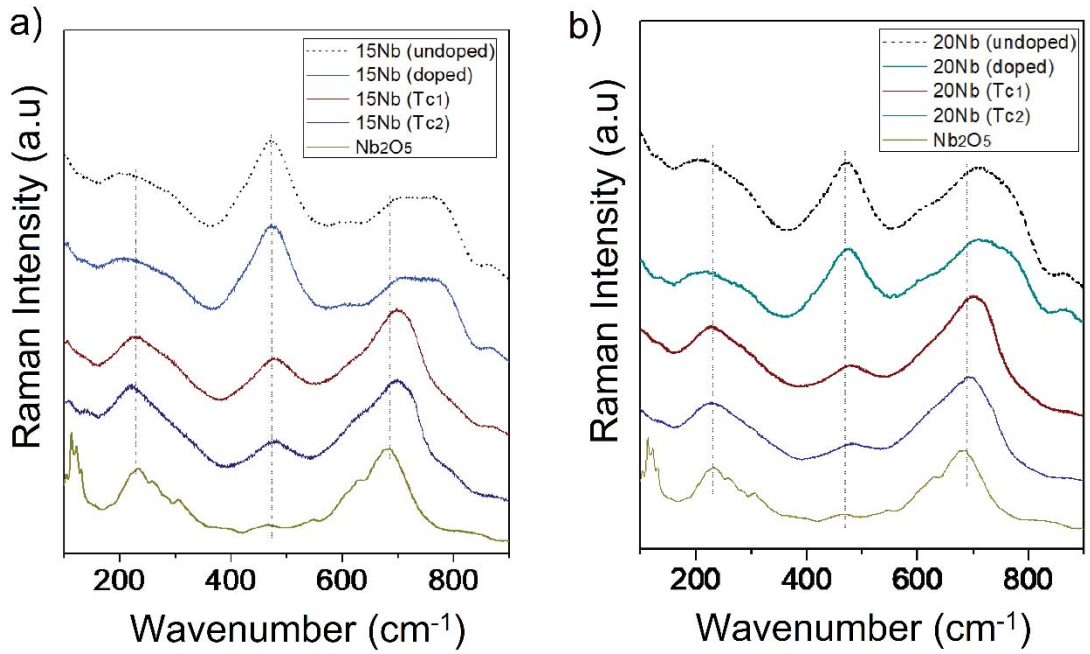

Figure S2. Raman spectra of undoped and Eu^{3+}-doped alkali niobium germanate glasses and respective glass-ceramics (a) 15Nb and (b) 20Nb; and crystalline reference Nb_2O_5.

^{93}Nb MAS NMR data

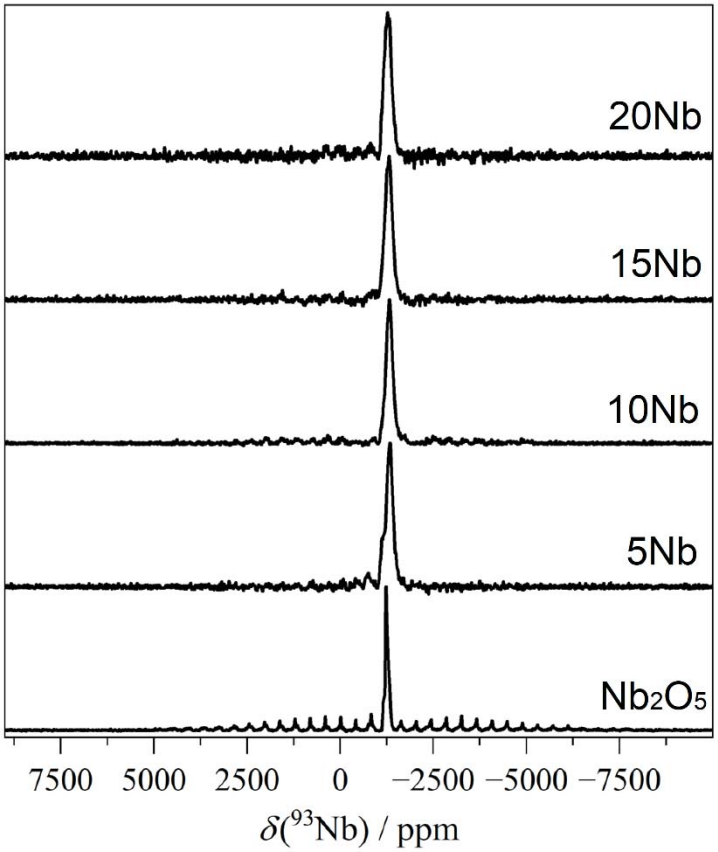

Figure S3*:* Full ^{93}Nb MAS NMR spectra of Eu^{3+}-doped alkali niobium germanate glasses and Nb_2O_5. Lineshape deconvolutions of the central-transition are shown in Figure 1.a.

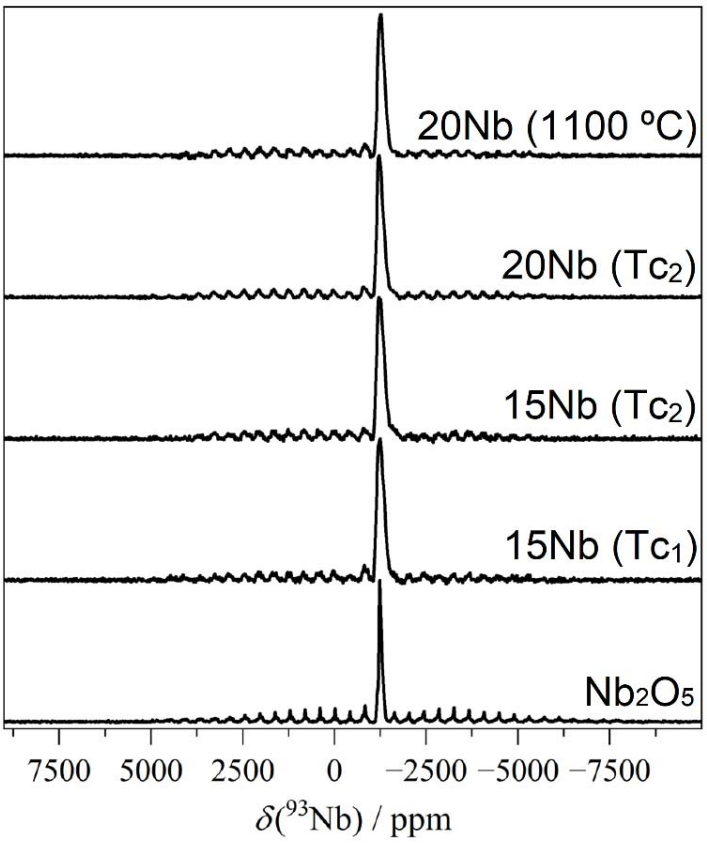

Figure S4*:* Full ^{93}Nb MAS NMR spectra of Eu^{3+}-doped alkali niobium germanate glasses and Nb2O5. Lineshape deconvolutions of the central-transition are shown in Figure 1.b.

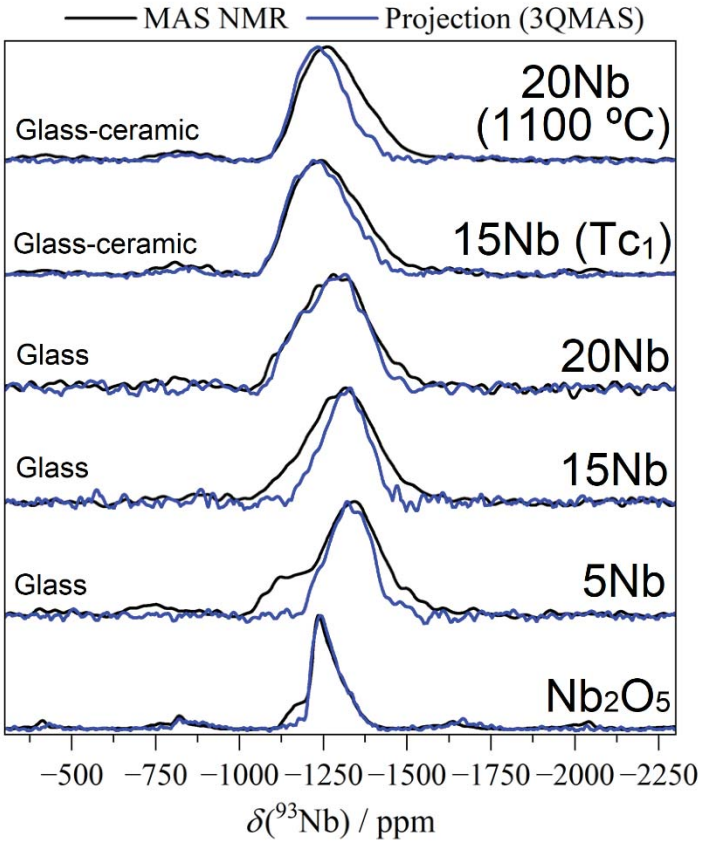

Figure S5: ^{93}Nb MAS NMR spectra (black line) and horizontal projections of 3QMAS NMR spectra of Eu^{3+}-doped alkali niobium germanate glasses, glass-ceramics (please refer to the text for details) and Nb_2O_5.

Graphical abstract

Click here to access/download;Figure;Graphical abstract.tif

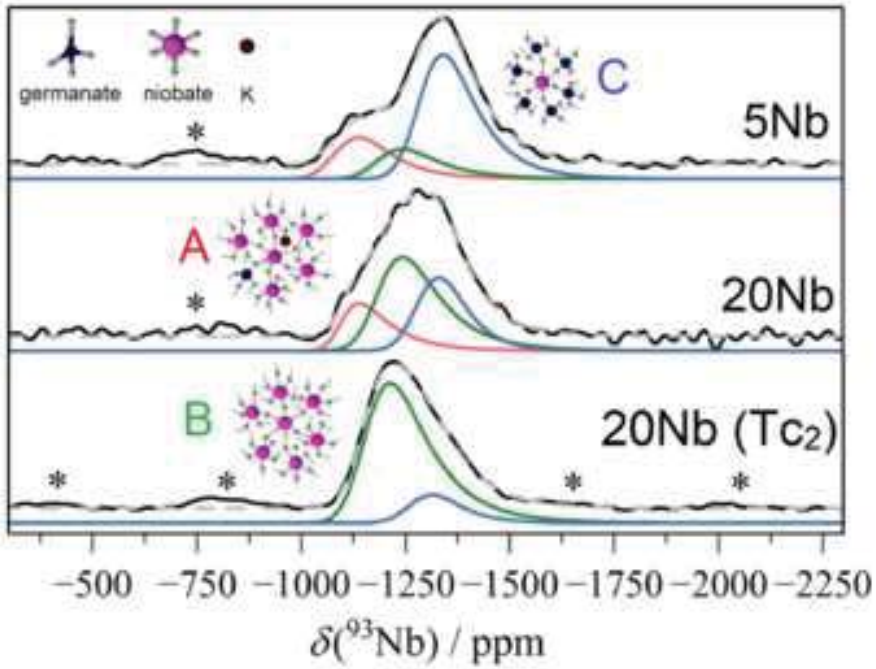

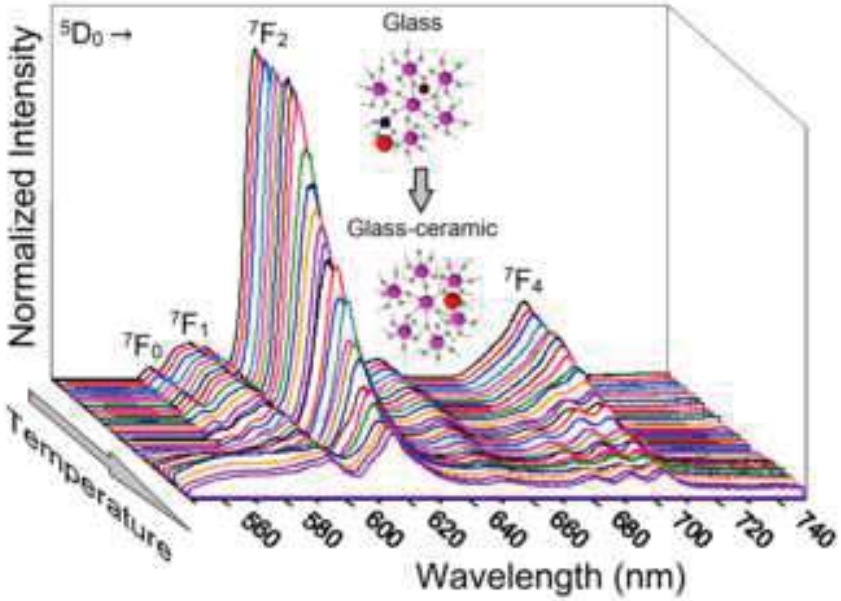

Declaration of interest statement

Date March 17, 2022

The authors whose names are listed immediately below certify that they have NO affiliations with or involvement in any organization or entity with any financial interest (such as honoraria; educational grants; participation in speakers' bureaus; membership, employment, consultancies, stock ownership, or other equity interest; and expert testimony or patent-licensing arrangements), or non-financial interest (such as personal or professional relationships, affiliations, knowledge or beliefs) in the subject matter or materials discussed in this manuscript.

Lia Mara Marcondes

Henrik Bradtmüller

Sabrina Nicoleti Carvalho dos Santos

Lucas Konaka Nolasco

Cleber Renato Mendonça

Silvia Helena Santagneli

Gael Yves Poirier

Marcelo Nalin

Lia Mara Marcondes

Institute of Chemistry, Sao Paulo State University - UNESP,
Araraquara, SP, Brazil
lia-marcondes@hotmail.com

Figure 1

Click here to access/download;Figure;Figure 1.tif

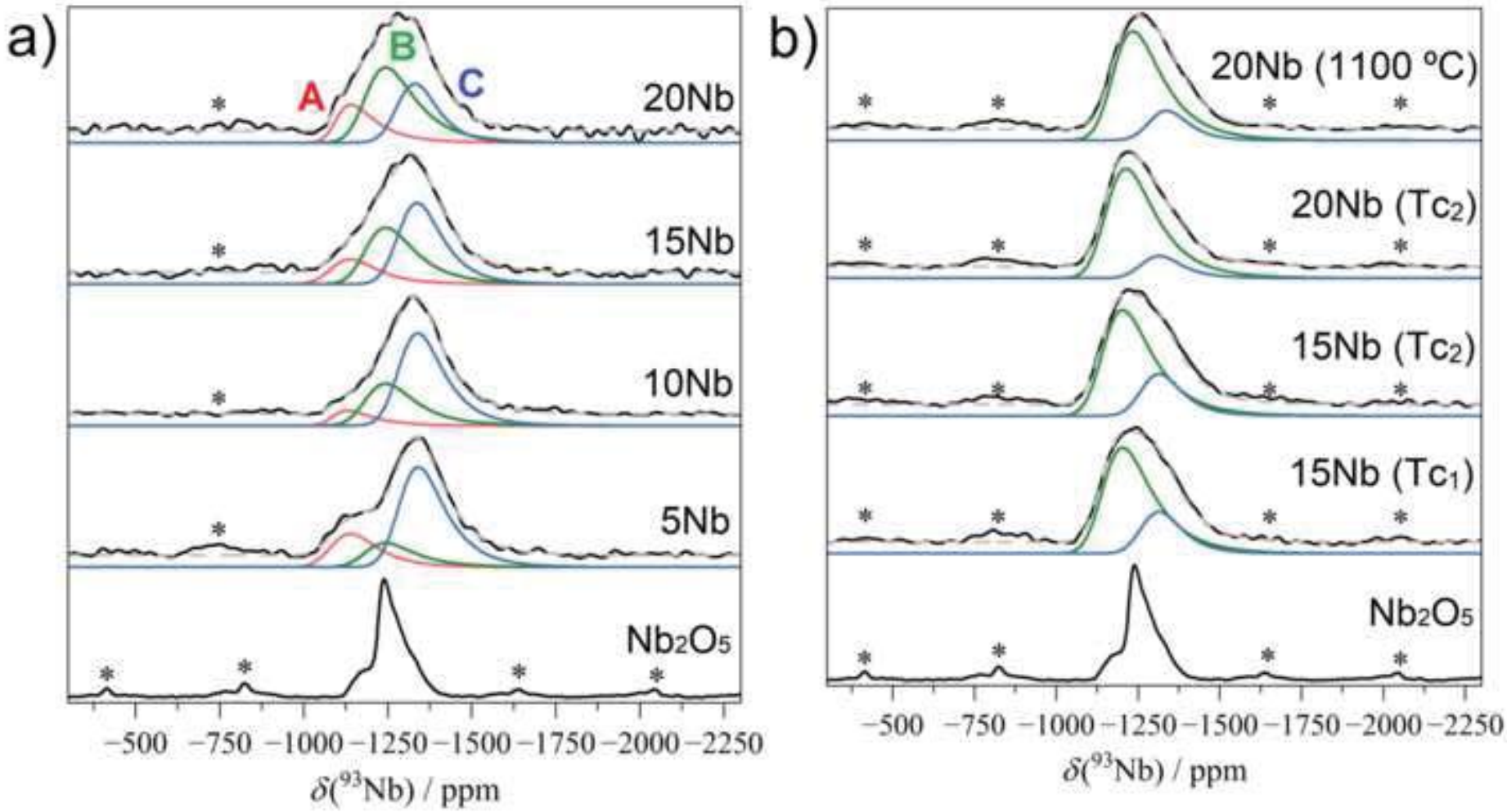

Figure 2

Click here to access/download;Figure;Figure 2.tif

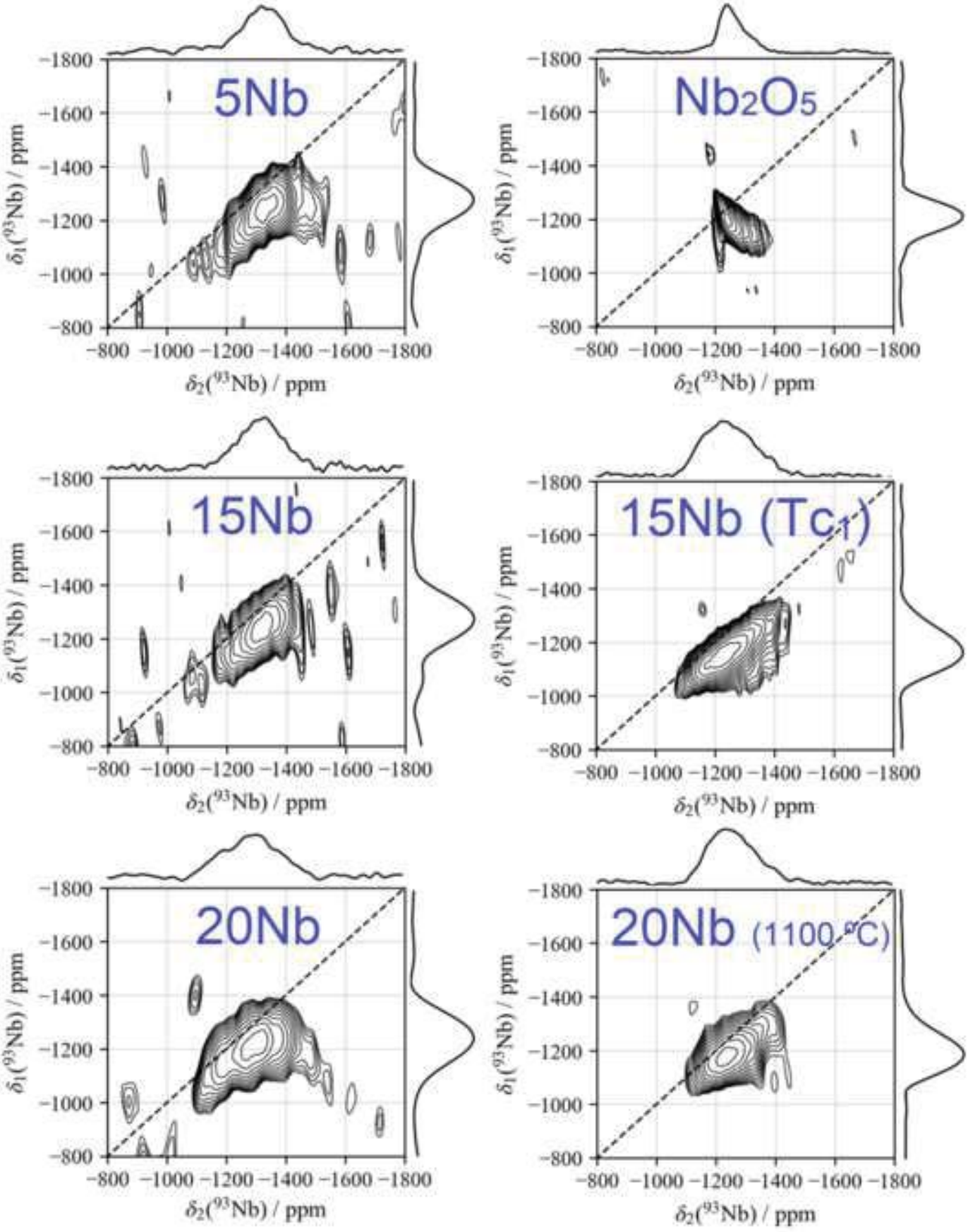

Figure 3

Click here to access/download;Figure;Figure 3.tif

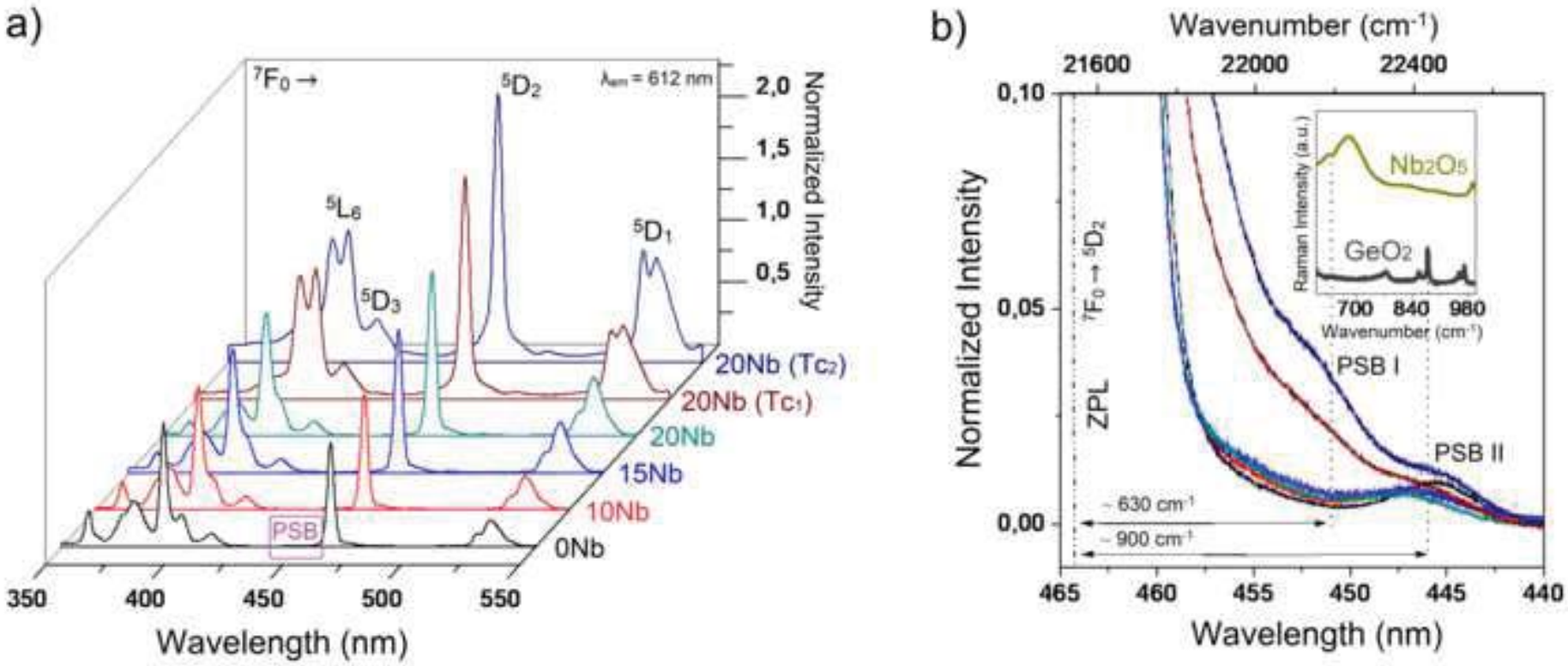

Figure 4

Click here to access/download;Figure;Figure 4.tif

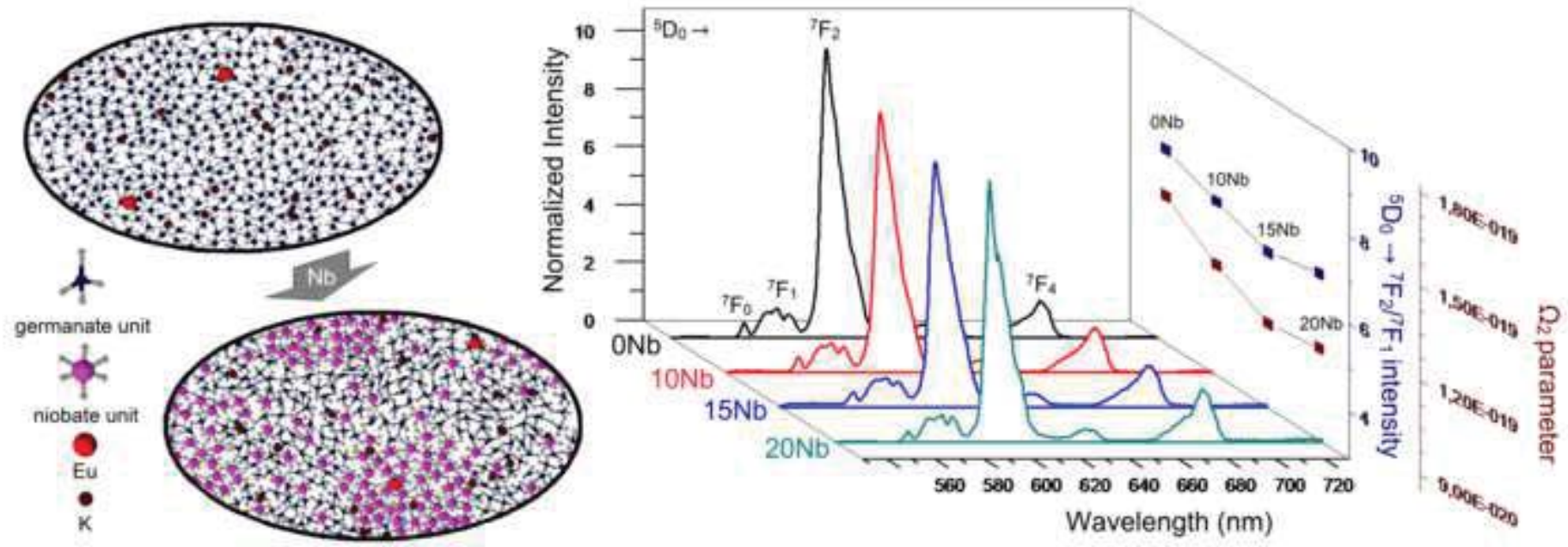

Figure 5

Click here to access/download;Figure;Figure 5.tif

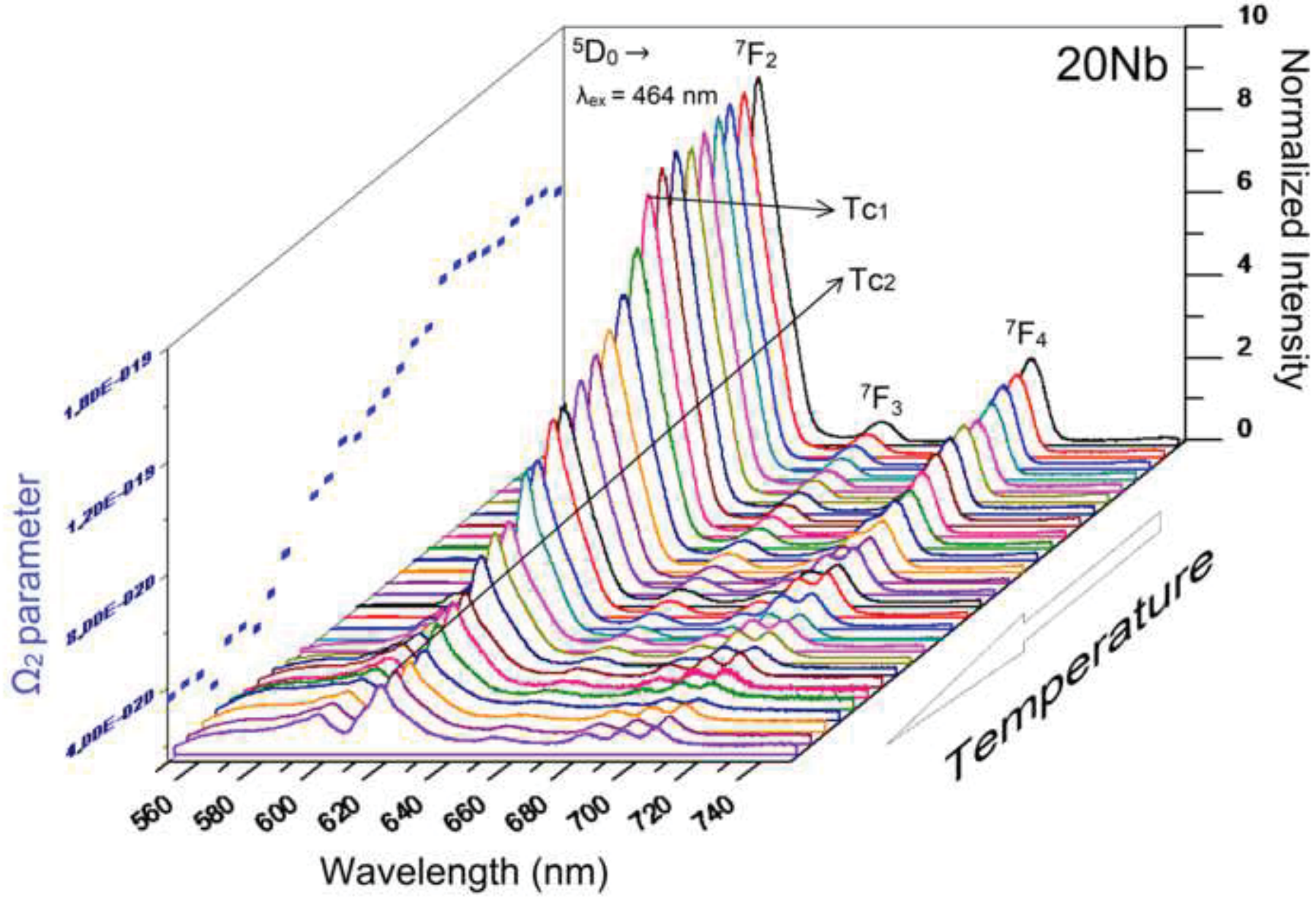

Figure 6

Click here to access/download;Figure;Figure 6.tif

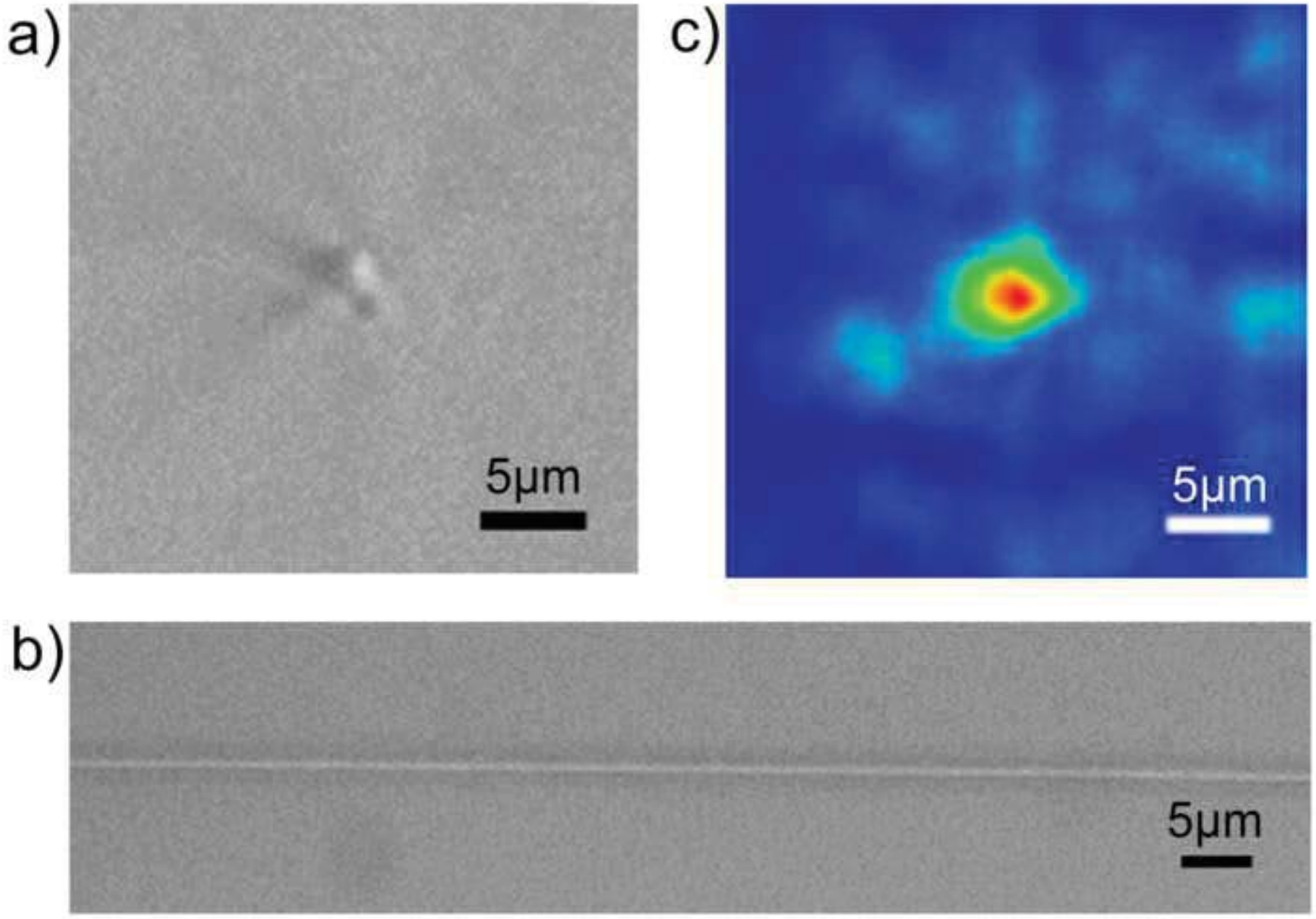

Figure S1

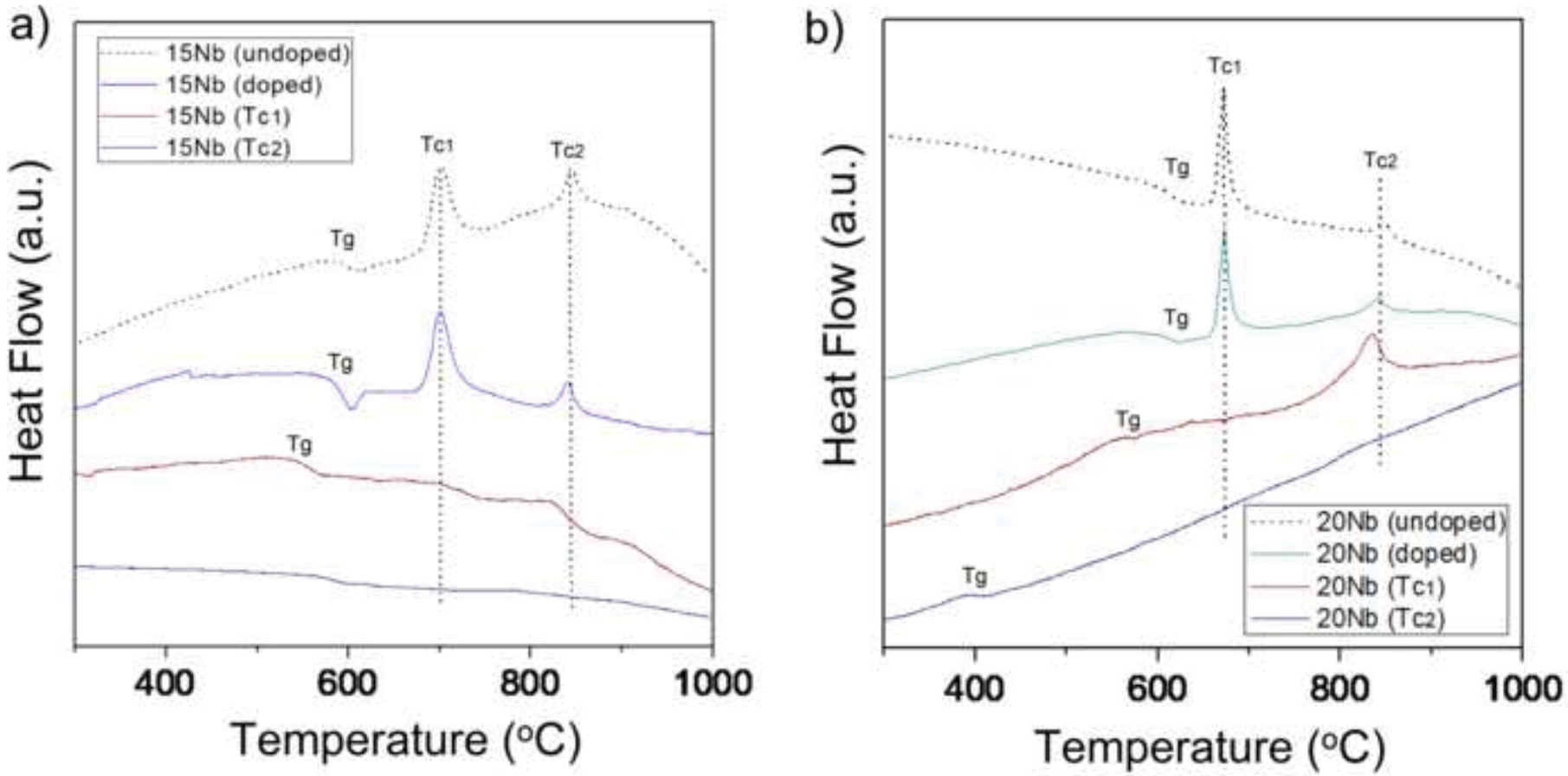

Figure S2

Click here to access/download;Figure;S2.tif

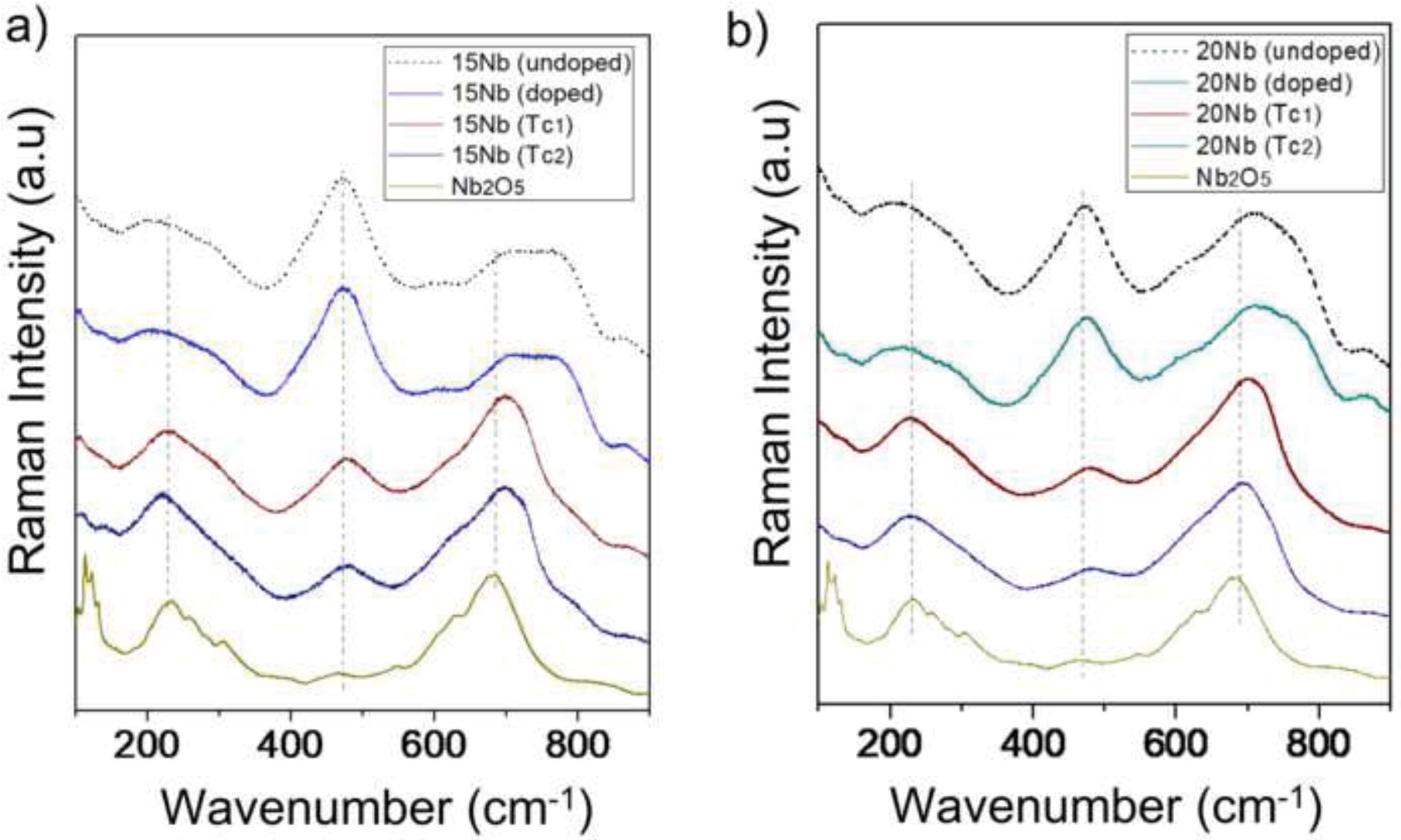

Figure S3

Click here to access/download;Figure;S3.tif

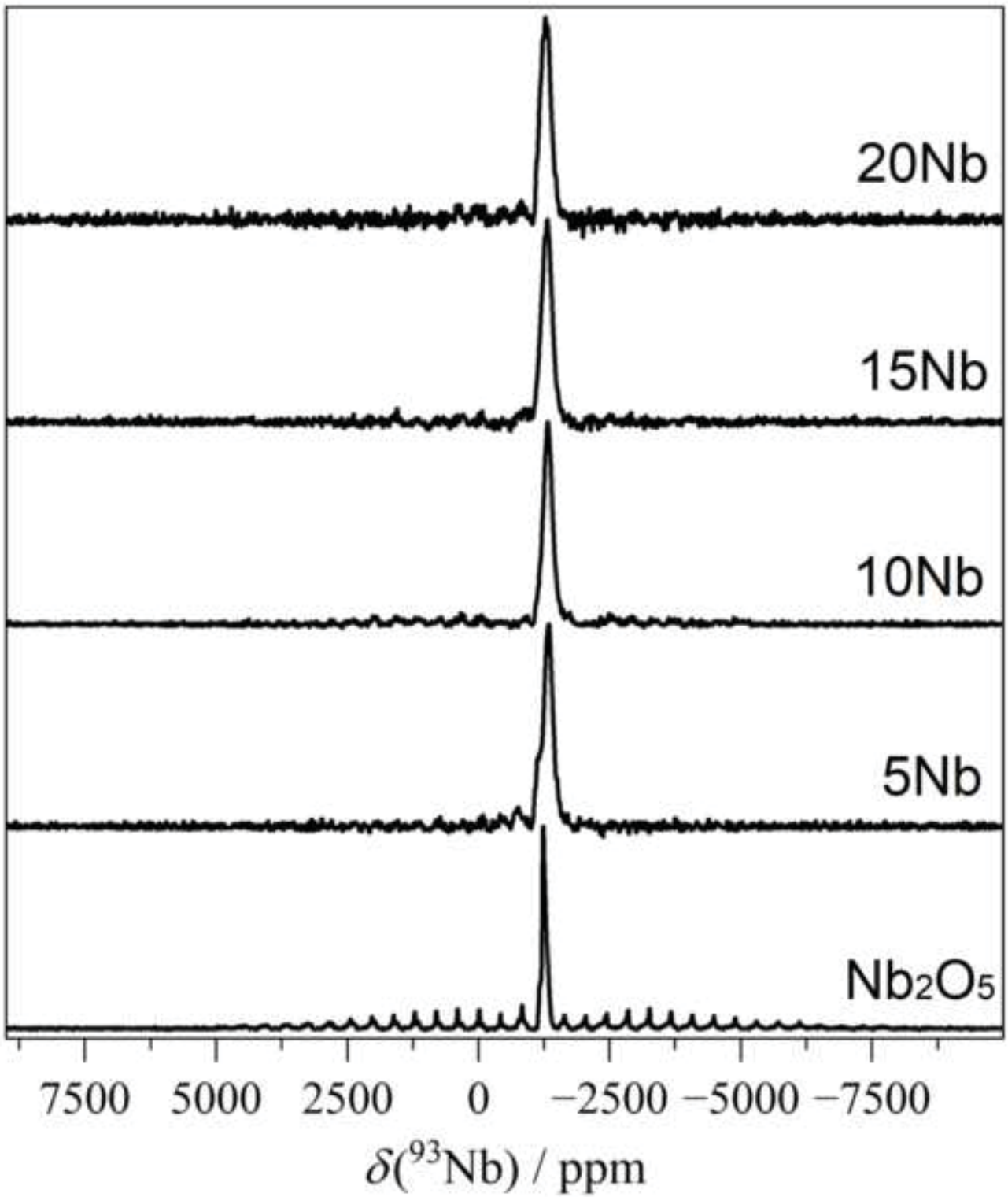

Figure S4

Click here to access/download;Figure;S4.tif

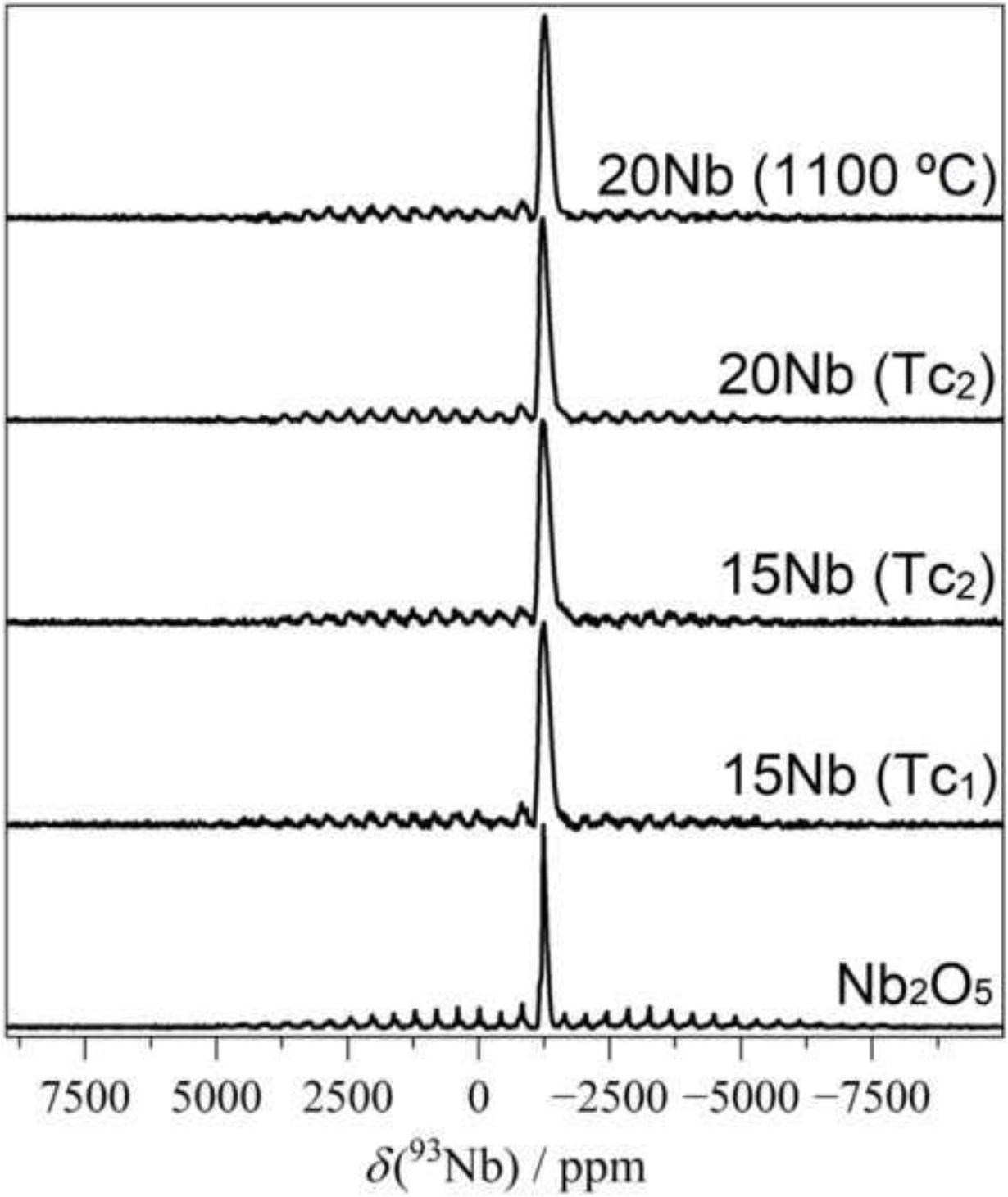

Figure S5

Click here to access/download;Figure;S5.tif